doi:10.1093/brain/awq349 Brain 2011: 134; 301–317 | 301

BRAIN
A JOURNAL OF NEUROLOGY

OCCASIONAL PAPER

Positron emission tomography imaging and clinical progression in relation to molecular pathology in the first Pittsburgh Compound B positron emission tomography patient with Alzheimer's disease

Ahmadul Kadir,[1,*] Amelia Marutle,[1,*] Daniel Gonzalez,[1] Michael Schöll,[1] Ove Almkvist,[1,2] Malahat Mousavi,[1] Tamanna Mustafiz,[1] Taher Darreh-Shori,[1] Inger Nennesmo[3] and Agneta Nordberg[1,2]

1 Department of Neurobiology, Care Sciences and Society, Karolinska Institutet, Karolinska University Hospital Huddinge, Stockholm, Sweden
2 Department of Geriatric Medicine, Karolinska University Hospital Huddinge, Stockholm, Sweden
3 Department of Pathology, Karolinska University Hospital Huddinge, Stockholm, Sweden

*These authors contributed equally to this work.

Correspondence to: Prof. Agneta Nordberg, MD, PhD,
Karolinska Institutet,
Department of Neurobiology,
Care Sciences and Society,
Division of Alzheimer Neurobiology,
Karolinska University Hospital Huddinge,
Novum Floor-5,
S-14186 Stockholm, Sweden
E-mail: agneta.k.nordberg@ki.se

The accumulation of β-amyloid in the brain is an early event in Alzheimer's disease. This study presents the first patient with Alzheimer's disease who underwent positron emission tomography imaging with the amyloid tracer, Pittsburgh Compound B to visualize fibrillar β-amyloid in the brain. Here we relate the clinical progression, amyloid and functional brain positron emission tomography imaging with molecular neuropathological alterations at autopsy to gain new insight into the relationship between β-amyloid accumulation, inflammatory processes and the cholinergic neurotransmitter system in Alzheimer's disease brain. The patient underwent positron emission tomography studies with ^{18}F-fluorodeoxyglucose three times (at ages 53, 56 and 58 years) and twice with Pittsburgh Compound B (at ages 56 and 58 years), prior to death at 61 years of age. The patient showed a pronounced decline in cerebral glucose metabolism and cognition during disease progression, while Pittsburgh Compound B retention remained high and stable at follow-up. Neuropathological examination of the brain at autopsy confirmed the clinical diagnosis of pure Alzheimer's disease. A comprehensive neuropathological investigation was performed in nine brain regions to measure the regional distribution of β-amyloid, neurofibrillary tangles and the levels of binding of ^{3}H-nicotine and ^{125}I-α-bungarotoxin to neuronal nicotinic acetylcholine receptor subtypes, ^{3}H-L-deprenyl to activated astrocytes and ^{3}H-PK11195 to microglia, as well as butyrylcholinesterase activity. Regional *in vivo* ^{11}C-Pittsburgh Compound B-positron emission tomography retention positively correlated with ^{3}H-Pittsburgh Compound B binding, total insoluble β-amyloid, and β-amyloid plaque distribution, but not with the number of neurofibrillary tangles measured at autopsy. There was a negative correlation between regional fibrillar β-amyloid and levels of ^{3}H-nicotine binding. In addition, a positive correlation was found

Received June 30, 2010. Revised October 13, 2010. Accepted October 14, 2010. Advance Access publication December 13, 2010

between regional ^{11}C-Pittsburgh Compound B positron emission tomography retention and ^{3}H-Pittsburgh Compound B binding with the number of glial fibrillary acidic protein immunoreactive cells, but not with ^{3}H-L-deprenyl and ^{3}H-PK-11195 binding. In summary, high ^{11}C-Pittsburgh Compound B positron emission tomography retention significantly correlates with both fibrillar β-amyloid and losses of neuronal nicotinic acetylcholine receptor subtypes at autopsy, suggesting a closer involvement of β-amyloid pathology with neuronal nicotinic acetylcholine receptor subtypes than with inflammatory processes.

Keywords: Alzheimer's disease; autopsy brain; ^{11}C-PIB positron emission tomography; inflammation; nicotinic acetylcholine receptors

Abbreviations: Aβ = β-amyloid; ^{3}H-PIB = ^{3}H-Pittsburgh Compound B; ^{11}C-PIB = ^{11}C-Pittsburgh Compound B; ^{18}F-FDG = ^{18}F-Fluorodeoxyglucose; PET = Positron emission tomography

Introduction

The underlying pathology of Alzheimer's disease is believed to precede the onset of clinical symptoms by many years (Thal *et al*., 2002). It has been hypothesized that the formation and accumulation of β-amyloid (Aβ) in the Alzheimer's disease brain triggers a cascade of neurodegenerative events, including inflammatory processes, oxidative stress, neurofibrillary tangles, neuronal network dysfunction with synaptic loss and neurotransmitter deficits (Braak and Braak, 1991; Nordberg, 2001; Thal *et al*., 2002; Ingelsson *et al*., 2004; Mattson, 2004; Price *et al*., 2009), which are manifested clinically by progressive impairment of cognitive functions. Previously, a definite diagnosis of Alzheimer's disease was considered only possible by post-mortem histopathological analysis of the brain; however, the development of new biomarkers including the amyloid positron emission tomography (PET) tracer Pittsburgh Compound B (^{11}C-PIB) for visualizing fibrillar Aβ, has created new possibilities for early detection of brain impairments.

Several ^{11}C-PIB PET studies in different cohorts of patients have shown a consistent high load of fibrillar Aβ in large parts of the Alzheimer's disease brain compared to healthy controls and other forms of dementia (Nordberg *et al*., 2010). Longitudinal amyloid imaging studies in subjects with mild cognitive impairment and Alzheimer's disease have suggested that the fibrillar Aβ levels in the brain reach a plateau early on and remain stable during the disease progression, whereas neurodegeneration and clinical decline measured by ^{18}F-fluorodeoxyglucose (^{18}F-FDG), MRI and cognitive tests accelerate and proceed independently of amyloid accumulation (Engler *et al*., 2006; Forsberg *et al*., 2008, 2010; Jack *et al*., 2009; Scheinin *et al*., 2009; Furst *et al*., 2010; Kadir *et al*., 2010). It has also been shown that the retention of ^{11}C-PIB *in vivo* correlates well with autopsy measures of Aβ deposition in the Alzheimer's disease brain, but not with tau (Ikonomovic *et al*., 2008).

We aimed to understand the relationship between clinical and pathological interactive mechanisms by investigating fibrillar Aβ accumulation, inflammatory processes and the cholinergic neurotransmitter system in an Alzheimer's disease brain, because these may be validated as PET biomarkers to reflect early changes as well as disease progression.

A 56-year-old female patient with Alzheimer's disease volunteered in February 2002 for the first ^{11}C-PIB PET scan in the world (Klunk *et al*., 2004). The patient died in August 2007, 35 months after having participated in a second ^{11}C-PIB PET scan, in August 2004. The results from the clinical longitudinal cognitive assessments as well as the repeated ^{11}C-PIB and ^{18}F-FDG PET imaging scans were assessed in relation to the autopsy data for Aβ plaques and neurofibrillary tangle distribution, as well as other pathological markers known to affect brain network function, including markers of inflammation (activated microglia and astrocytes) and neuronal nicotinic acetylcholine receptor losses in different brain regions.

Case history and methods

Clinical description

In 1999, a female patient aged 53 years, was referred from a local hospital to the Department of Geriatric Medicine at Karolinska University Hospital Huddinge, Stockholm, Sweden. The patient had no known family history of dementia or other neurodegenerative diseases. In addition to the patient's own experience of cognitive problems a couple of years prior, during her occupation as a nurse, relatives confirmed difficulties with memory, both at work and at home. The patient underwent a thorough clinical investigation including medical history, cognitive screening, physical and neurological examinations as well as laboratory blood tests, including apolipoprotein E genotyping, neuropsychological assessment, lumbar puncture, electroencephalography (EEG), computed tomography (CT) and single photon emission computed tomography imaging (SPECT). The CT scan was normal; however, the SPECT scan showed decreased cerebral perfusion bilateral in the parietal cortex, predominantly on the left side. EEG investigation showed decreased alpha amplitude as well as theta/delta activity. Analysis of cerebrospinal fluid (CSF) biomarkers revealed pathological values with Aβ42 438 pmol/ml (<450 pmol/ml is abnormal) and tau 1180 pmol/ml (>400 pmol/ml is abnormal). The patient was an ApoE ε 4/4 carrier. The clinical diagnosis of Alzheimer's disease was made in accordance with the criteria from the workgroup formed by the National Institute of Neurological and Communication Disorders and Stroke-Alzheimer's disease and Related Disorders Association (NINCDS-ADRDA) (McKhann *et al*., 1984). The patient received treatment with the cholinesterase inhibitor rivastigmine (12 mg daily) and at a more advanced stage of the disease, she was also treated with memantine (20 mg daily). The patient was clinically assessed (by A.N.), every 6 months from

1999 to 2007. The patient lived at home with her family until she was admitted to a nursing home, 4 months prior to her death at 61 years of age. Consent from next of kin was given for research studies prior to autopsy.

Neuropsychological assessments

An experienced neuropsychologist (O.A.) performed cognitive assessments at regular intervals during 1999–2006. These neuropsychological tests included a global scale test, i.e. the full-scale intelligence quotient (FSIQ) test, as well as cognitive tests used to assess specific domains such as verbal abilities (similarities and information), visuospatial abilities (block design and Rey–Osterrieth copying), short-term memory (digit span and corsi span), episodic memory (Rey auditory verbal learning and retention after 30 min; Rey-Osterrieth Retention after 30 min) and attention and executive function (Digit Symbol and Trail Making Test A and B). Detailed information regarding the above-mentioned tests has been described previously (Almkvist and Tallberg, 2009). In order to make comparisons between various neuropsychological test results, all cognitive raw scores were *z*-transformed by using reference data from healthy adults at the Geriatric Clinic, Karolinska University Hospital Huddinge (Bergman *et al*., 2007).

Magnetic resonance imaging

MRI was performed at the age of 53 using a 1.5 T scanner (Magnetom Vision Plus, Siemens, Germany) and included a T_1-weighted 3D magnetization-prepared rapid gradient echo sequence (MP-RAGE), repetition time: 11.4 ms, effective echo time: 4.4 ms, flip angle: 10°, slice thickness: 2.5 mm.

Medial temporal lobe atrophy was assessed visually according to the Scheltens scale (Scheltens *et al*., 1992) on coronal 3D magnetization-prepared rapid gradient echo sequence slices perpendicular to the anterior commissure and the posterior commissure line at the mid-level of the brainstem after having amygdala in front.

The medial temporal lobe atrophy scale ranges from 0 (no atrophy) to 4 (severe atrophy) and takes into account the width of the choroidal fissure, the height of the hippocampus and the width of the temporal horn of the lateral ventricle. Left and right medial lobe atrophy was rated separately. A trained rater, who was blinded to the clinical information of this case, rated the medial temporal lobe atrophy.

Positron emission tomography

The PET examinations with ^{18}F-FDG and ^{11}C-PIB were performed at Uppsala Academic Hospital, Sweden. Production of ^{18}F-FDG and ^{11}C-PIB was carried out according to standard manufacturing processes and synthesis of ^{11}C-PIB was performed by means of a previously described method (Mathis *et al*., 2003; Klunk *et al*., 2004).

Positron emission tomography scanning: ^{18}F-fluorodeoxyglucose

From 1999 to 2004, the patient underwent three ^{18}F-FDG PET scans at ages 53, 56 and 58 years. The PET scans were performed using Siemens ECAT EXACT HR+ scanners (CTI PET-Systems, Inc., Knoxville TN, USA) with an axial field of view of 155 mm, providing 63 contiguous 2.46 mm slices with 5.6 mm transaxial and 5.4 mm axial resolution. The patient was scanned under resting condition after fasting for 4 h. The orbito-meatal line was used to centre the heads of the subject. The data were acquired in a 3D mode. The administered mean ^{18}F-FDG tracer dose was 210 MBq. The scanner protocol for transmission, emission and reconstruction has been described previously (Klunk *et al*., 2004; Engler *et al*., 2006).

Parametric maps of regional cerebral glucose metabolism were generated by means of the Patlak method using the time course of the tracer in the arterialized venous plasma samples as an input function (Patlak *et al*., 1983). The frames from 20 to 60 min and a lumped constant of 0.418 were used to generate the parametric maps of regional cerebral glucose metabolism. All values are expressed in μmol/min/100 g.

Positron emission tomography scanning: ^{11}C-Pittsburgh Compound B

In February 2002, the patient underwent the first ^{11}C-PIB PET scan at 56 years of age, with an additional ^{11}C-PIB PET scan performed in August 2004, at 58 years of age. The protocols for the ^{11}C-PIB PET examinations, including the scanner protocol for transmission, emissions and reconstructions are described in detail in the above-mentioned studies (Klunk *et al*., 2004; Engler *et al*., 2006). The ^{11}C-PIB examinations were performed using a Siemens ECAT EXACT HR+ scanner (CTI PET-systems Inc.), with an axial field of view of 155 mm, providing 63 contiguous 2.46 mm slices with a 5.6 mm transaxial and a 5.4 mm axial resolution. The mean tracer dose of ^{11}C-PIB was 320 MBq.

The ^{11}C-PIB retention data were calculated as standard uptake values as previously described in detail (Klunk *et al*., 2004) and were obtained in a late time interval (40–60 min).

Regions of interest

A set of standardized regions of interest was used to determine the inter-relation between PET data and cognitive tests and to compare the PIB scans 1 and 2. The region of interest placement procedure has been described in detail (Schöll *et al*., 2009). A computerized reorientation procedure developed in-house was used to align consecutive ^{18}F-FDG- and ^{11}C-PIB-PET images for accurate intra-comparison and application of regions of interest (Andersson and Thurfjell, 1997). The ^{18}F-FDG images were realigned to the first ^{18}F-FDG image and the ^{11}C-PIB images at baseline and follow-up were co-realigned using the respective ^{18}F-FDG images as templates. To compare the baseline and follow-up ^{11}C-PIB scans, the regional ^{11}C-PIB retention values were normalized to the corresponding uptake in a cerebellar

reference region. The cerebellar cortex was chosen as the reference region because of its previously reported lack of Congo red- and thioflavin-S-positive plaques (Yamaguchi *et al*., 1989; Mirra *et al*., 1994).

Statistical parametric mapping methods

Voxel based analysis with statistical parametric mapping (SPM5) (Wellcome Department of Cognitive Neurology, Institute of Neurology, London, UK), which was implemented using Matlab 7.1 (MathWorks Inc., Sherborn, MA), was used to compare the regional cerebral glucose metabolism at the age of 53, 56 and 58 with a healthy control population [$n = 6$, mean age 67.3 ± 8.8 standard deviation (SD)]. All reconstructed PET images were spatially normalized into the Montreal Neurological Institute standard template (McGill University, Montreal, Canada) to remove inter-scan and inter-subject anatomical variability. Spatially normalized images were smoothed by convolution, using an isotropic Gaussian kernel with 8 mm full-width at half-maximum. Proportional scaling was used for global normalization. Voxel-wise two-sample *t*-test for comparison between-group (patient with Alzheimer's disease versus healthy controls) was computed at the three time points, with *P*-values uncorrected for multiple comparisons. The brain areas that showed glucose hypometabolism at a peak threshold of $P = 0.001$ (uncorrected) and an extent threshold of 50 voxels were investigated. For visualization of the *t*-score statistics (statistical parametric mapping *t*-map), the significant voxels were projected onto the 3D rendered brain thus allowing anatomical identification. The Montreal Neurological Institute coordinates of the local maximum of each cluster were converted into Talairach coordinates (Talairach and Tournoux, 1988).

Neuropathology and immunohistochemistry

The brain was obtained with a post-mortem delay of 17 h. At autopsy, small samples from nine regions of interest: the frontal, temporal, parietal and occipital cortices, the anterior and posterior part of the hippocampus, striatum, thalamus and the cerebellum were collected from the left hemisphere and frozen at −70°C. Coronal sections of the left hemisphere were frozen separately. The right half of the brain was fixed in 4% formaldehyde. Material for histopathological examination was collected according to the Brain Net Europe guidelines (Alafuzoff *et al*., 2006) after 3 weeks of fixation. Staining for pathological evaluation was performed on 5 mm thick formaldehyde fixed paraffin-embedded sections. Sections were routinely stained with haematoxylin and eosin, luxol fast blue, Bielschowsky silver stain and Congo red. The diagnostic evaluation was performed by an experienced clinical neuropathologist (I.N.).

For further characterization of the pathological lesions and for correlation with the PIB analysis, immunohistochemistry was performed on sections mounted on SuperFrost® Slides (Thermo Scientific, Waltham, MA, USA). Pretreatment with formic acid (88%) for 10 min was carried out in connection with incubation with β-amyloid antibodies. Staining was performed using antibodies diluted in Bond™ primary antibody diluent (Vision BioSystems Limited, Newcastle upon Tyne, UK), specific for Aβ40 and Aβ42 (BioSource, USA), Aβ clone 6F/3D (DakoCytomation, Denmark), Aβ 6E10, Aβ 4G8 (Chemicon International, Temecula, USA), glial fibrillary acidic protein (DakoCytomation, Denmark) and tau AT8 (Innogenetics, Belgium). A summary of the primary antibodies used is shown in Supplementary Table 1. Negative controls consisted of sections incubated in the absence of a primary antibody. All sections were counterstained with haematoxylin.

The semiquantitative analysis was assessed by the frequency of senile plaques, neurofibrillary tangles and astrocytes in areas of maximum density as described previously (Mirra *et al*., 1991; Cummings *et al*., 1996). The densities were expressed as the absence of immunoreactivity (−), rare number of profiles (+), sparse number of profiles (+ +), moderate number of profiles (+ + +), frequent profiles (+ + + +) and extensive or widespread profiles (+ + + + +) (Table 1). In each of the nine regions of interest, the number of senile plaques, neurofibrillary tangles and astrocytes was counted and the total number was averaged from each region of study. All sections were imaged sequentially under light microscopy and counted in ×200 magnification during a

Table 1 Semi-quantitative immunohistochemical assessments of Aβ plaques, neurofibrillary tangles and reactive astrocytes in autopsy brain of the patient with Alzheimer's disease

Regions	Aβ (1–40)		Aβ (1–42)		Aβ (6F/3D)		Aβ (4G8) (EC)		Aβ (4G8) (IC)		Aβ (6E10)		NFTs (tau AT8)		Astrocytes (GFAP)	
	Count	Score	Count	Score	Count	Score	Count	Score	Count	Score	Count	Score	Count	Score	Count	Score
Frontal	20	+ +	61	+ + + +	69	+ + + +	61	+ + + +	61	+ + +	26	+ +	13	+	74	+ + + + +
Temporal	8	+	41	+ + +	57	+ + +	53	+ + +	65	+ + +	9	+	29	+ + +	62	+ + + + +
Parietal	20	+ +	92	+ + + + +	99	+ + + + +	70	+ + + +	43	+ + +	19	+	3	+	62	+ + + + +
Occipital	29	+ +	44	+ + +	54	+ + +	66	+ + + +	54	+ + +	23	+ +	3	+	51	+ + + +
Hippo A	7	+	13	+	12	+	20	+ +	106	+ + + +	5	+	69	+ + + + +	39	+ + +
Hippo P	7	+	9	+	14	+	14	+	158	+ + + + +	4	+	50	+ + + +	39	+ + +
Putamen	3	+	34	+ +	14	+	23	+ +	106	+ + + +	0	−	4	+	31	+ + +
Thalamus	3	+	9	+	5	+	14	+	35	+ +	4	+	14	+ +	38	+ + +
Cerebellum	0	−	1	+	12	+	17	+	26	+	0	−	0	−	2	+

EC = extracellular; GFAP = glial fibrillary acidic protein; Hippo A = hippocampus anterior; Hippo P = hippocampus posterior; IC = intracellular.
Score: (−) absent, (+) rare, (+ +) sparse, (+ + +) moderate, (+ + + +) frequent, (+ + + + +) extensive.

single session to prevent changes in illumination or video camera setup.

Measurement of β-amyloid levels

Soluble and insoluble Aβ40 and Aβ42 were quantified in brain homogenates of frozen tissue (150–200 μg) using commercial enzyme-linked immunosorbent assay kits (Signal Select™ Human β-amyloid 1–40 and 1–42 from BioSource International Inc., Camarillo, CA, USA) according to a previous protocol (Hellstrom-Lindahl *et al*., 2004). Levels of Aβ were expressed as pg/mg tissue.

Neurochemical binding and enzyme assays

Fresh-frozen autopsy tissue samples (grey matter) from the nine regions of interest were homogenized in cold 0.32 M sucrose containing protease inhibitors. The homogenates were aliquoted and frozen at −80°C until the binding assays were carried out.

Saturation binding with ^{3}H-Pittsburgh Compound B (^{3}H-PIB) was performed in homogenate tissue from the frontal cortex (100 μg tissue) by incubation with 0.2 to 300 nM ^{3}H-PIB (specific activity 68 Ci/mmol, custom synthesis, GE Healthcare, Germany). Non-specific binding was determined in the presence of 1 μM unlabelled PIB (Sigma-Aldrich). Saturation binding analysis revealed high-affinity binding for ^{3}H-PIB (K_d = 3.5 nM) and 1 nM ^{3}H-PIB was used in all subsequent measurements of high-affinity binding sites.

^{3}H-nicotine and ^{125}I-α-bungarotoxin binding to the two major neuronal nicotinic acetylcholine receptor subtypes in the brain (α4β2 and α7) as well as ^{3}H-PK11195 and ^{3}H-L-deprenyl binding to activated microglia cells and monoamine oxidase B present in activated astrocytes, was measured by incubating homogenates from the nine brain regions with ^{3}H-nicotine (5.0 nM, specific activity 75 Ci/mmol, NEN Life Science Products) (Marutle *et al*., 1998), ^{125}I-α-bungarotoxin (2 nM, specific activity 108.8 Ci/mmol, Perkin Elmer, Waltham, MA, USA) (Guan *et al*., 2001), ^{3}H-PK11195 (5.0 nM, specific activity 83.4 Ci/mmol, American Radiolabeled Chemicals, St Louis, MO, USA) (Kumlien *et al*., 1992) and ^{3}H-L-deprenyl (10 nM, specific activity 80 Ci/mmol, Larodan Fine Chemicals AB, Malmö, Sweden) (Jossan *et al*., 1991*a*). Specific binding values were expressed as fmol/mg tissue or fmol/mg protein. Butyrylcholinesterase activity was measured by using a modified Ellman's colorimetric assay as described by Darreh-Shori *et al*. (2006).

Analysis of *in vivo* and *in vitro* correlations

To match the regional autopsy values from the nine different regions of interest with the corresponding regional ^{11}C-PIB PET retention and ^{18}F-FDG PET uptake values, the corresponding regions of interest were first drawn in accordance with the Brain Net Europe guidelines (Alafuzoff *et al*., 2006) on the same MRI coronal levels with the necessary adjustments for exclusion of white matter. Thereafter, the regions of interest were copied onto the coregistered ^{11}C-PIB and ^{18}F-FDG-PET scans. Supplementary Figure 1 illustrates the placement of regions of interest on coronal hemispheres and how these regions of interest were used in the correlation analyses. Data from the last ^{11}C-PIB (standard uptake value) and ^{18}F-FDG PET (μmol/min/100g), 35 months prior to death, were used in correlations with data obtained from measurements performed in the autopsy brain tissue.

Statistical analysis

In sum, 43 correlations were performed across this entire study (^{11}C-PIB versus 12 parameters; ^{3}H-PIB versus 10 parameters; ^{18}F-FDG versus six parameters; and ^{3}H-L-deprenyl versus two parameters; glial fibrillary acidic protein immunoreactive cells versus seven parameters; ^{3}H-nicotine versus three parameters; ^{125}I-α-bungarotoxin versus three parameters). Correlation analyses were performed by using non-parametric Spearman's rank order correlation. Due to the explorative nature of the study and the low statistical power (as nine brain regions were used in the correlations), statistical Bonferroni correction for multiple comparisons yielding a significant level 0.0012 (0.05/43) was not carried out. The level of statistical significance was set at 0.05 (two-sided). This implies that the results should be interpreted with some caution.

In addition, stepwise regression analysis was performed to determine correlations between cognitive test performances and regional cerebral glucose metabolism as measured by ^{18}F-FDG PET in various brain areas during the progression of disease (age 53–58 years).

Results

Longitudinal study of cognition, ^{18}F-fluorodeoxyglucose uptake and ^{11}C-Pittsburgh Compound B retention by positron emission tomography

The first neuropsychological assessment of the patient with Alzheimer's disease, at 53 years of age, revealed significant cognitive impairment, particularly in visuospatial ability, short-term memory and executive functioning, while verbal ability was preserved (Fig. 1A). The mini-mental state examination score was 27 out of 30 during the first visit to the Geriatric Clinic at age 53, and progressively declined over the course of the disease with a score of 5 out of 30 during the last cognitive assessment at the age of 60 years. The pattern of decline in mini-mental state examination scores was best-fit to a curvilinear regression line (r = 0.97, Fig. 1B). Progressive decline was longitudinally observed in other cognitive tests such as global cognition, episodic memory and attention (Fig. 1C).

The MRI scan was performed as part of the clinical assessment at 53 years of age. No infarction or haemorrhage was noted. The patient had discrete bilateral parietal atrophy (Fig. 2A and B), and

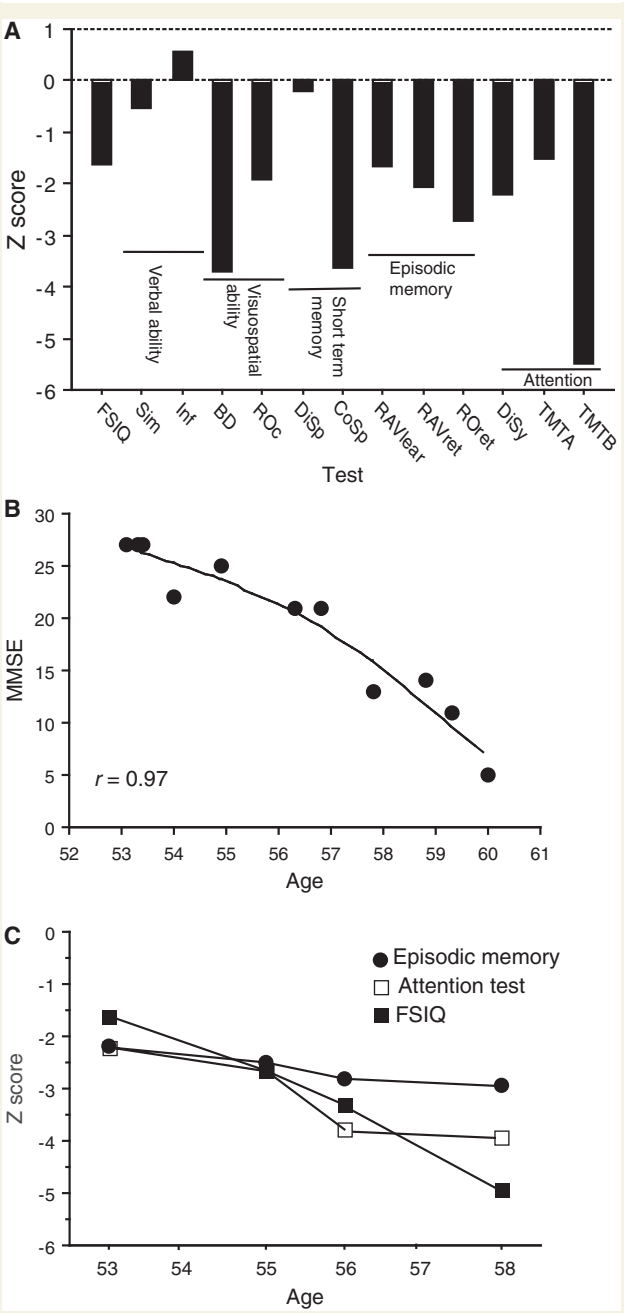

Figure 1 (**A**) Neuropsychological test performances presented as z-transformed raw scores in the patient with Alzheimer's disease at the age of 53 years. (**B**) Curvilinear regression ($r = 0.97$) between age (from 53 to 60 years) and mini-mental state examination (MMSE) score. (**C**) Longitudinal data on three cognitive subtests presented as *z*-transformed raw scores. Closed circles = episodic memory; open squares = digit symbol attention test; filled squares = full-scale intelligence quotient test (FSIQ); BD = block design; Cosp = corsi span; Disp = digit span; Disy = digit symbol; Inf = information; RAVlear = Rey auditory verbal learning; RAVret = Rey auditory verbal retention; ROc = Rey–Osterrieth copying; ROret = Rey–Osterrieth retention; Sim = similarities; TMT A and B = trail making A and B.

for the hippocampus, the medial temporal lobe atrophy score was 1 (left side) and 1–2 (right side) (Fig. 2C).

Voxel-based analysis of ^{18}F-FDG-PET using statistical parametric mapping was performed to visualize the decline in regional cerebral glucose metabolism in the patient, compared with that from a group of healthy control subjects. The 3D-rendered image of the voxel mapping showed significant decreases in regional cerebral glucose metabolism in certain brain regions (right hemisphere: superior parietal lobule, inferior parietal lobule, precuneus, superior frontal gyrus, inferior frontal gyrus, superior temporal gyrus, parahippocampal gyrus and fusiform gyrus; left hemisphere: inferior parietal lobule, superior frontal gyrus; all $P = 0.001$ uncorrected, $k = 50$) at the first ^{18}F-FDG-PET scan at 53 years of age (Fig. 3A). In line with the cognitive decline, there was also a pronounced decrease in regional cerebral glucose metabolism with disease progression as illustrated with voxel-based statistical parametric mapping analysis at 56 and 58 years of age, compared with the healthy control group (Fig. 3B and C).

By using the stepwise regression analysis, we observed that regional cerebral glucose metabolism, in three areas of the brain that are affected early on in the disease course (medial temporal, posterior cingulate and lower parietal), significantly correlated ($P < 0.05$) with test scores for attention, episodic memory and FSIQ during progression of the disease (Fig. 4).

The first ^{11}C-PIB scan at 56 years of age (mini-mental state examination 21/30) showed high ^{11}C-PIB retention especially in the frontal, parietal, parietotemporal, temporal, posterior cingulate and in the striatum (Fig. 5A and B). At 2 year follow-up (mini-mental state examination 13/30), the cortical ^{11}C-PIB retention remained high and relatively unchanged (Fig. 5A and B), in contrast to the continuous decline observed in regional cerebral glucose metabolism paralleling the decline in cognitive performance (Figs 1 and 3).

Semi-quantitative immunohistochemical assessment of neuropathology at autopsy

The brain weighed 1100g. Macroscopic inspection showed a widening of sulci and cortical and hippocampal atrophy. The anterior part of the hippocampus had a particularly reduced size and the ventricles were slightly enlarged. The histopathological examination revealed a pure Alzheimer's disease pathology (Braak stage 6, definite CERAD) confirming the clinical diagnosis of Alzheimer's disease. Congo red staining showed several positive vessels in the leptomeninges and the cortex, consistent with cerebral amyloid angiopathy.

Immunohistochemical assessment of the regional distribution of different types of Aβ-containing plaques showed varied staining patterns with Aβ antibodies with different epitope specificity. More plaques were stained with antibodies for Aβ1–42, 4G8 (reactive to amino acid residue 17–24) and 6F/3D (residue 8–17) when compared with antibodies for Aβ1–40 and 6E10 (residue 1–17) (Fig. 6A–E). 4G8 labelled both plaques and intracellular Aβ deposits in all the regions studied. A high distribution of intracellular Aβ was detected by 4G8 in the hippocampus (score

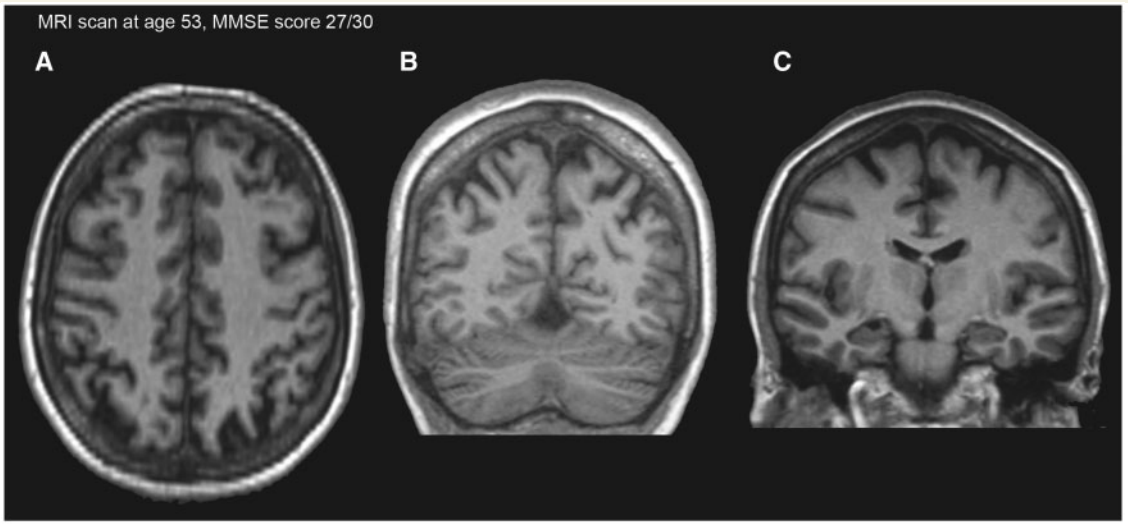

Figure 2 T_1-weighted MRI scan at the transaxial (**A**) and coronal (**B**) sections showing the bilateral parietal atrophy. MRI scan at the coronal section showing the medial temporal lobe atrophy score for the hippocampus (**C**). MMSE = mini-mental state examination.

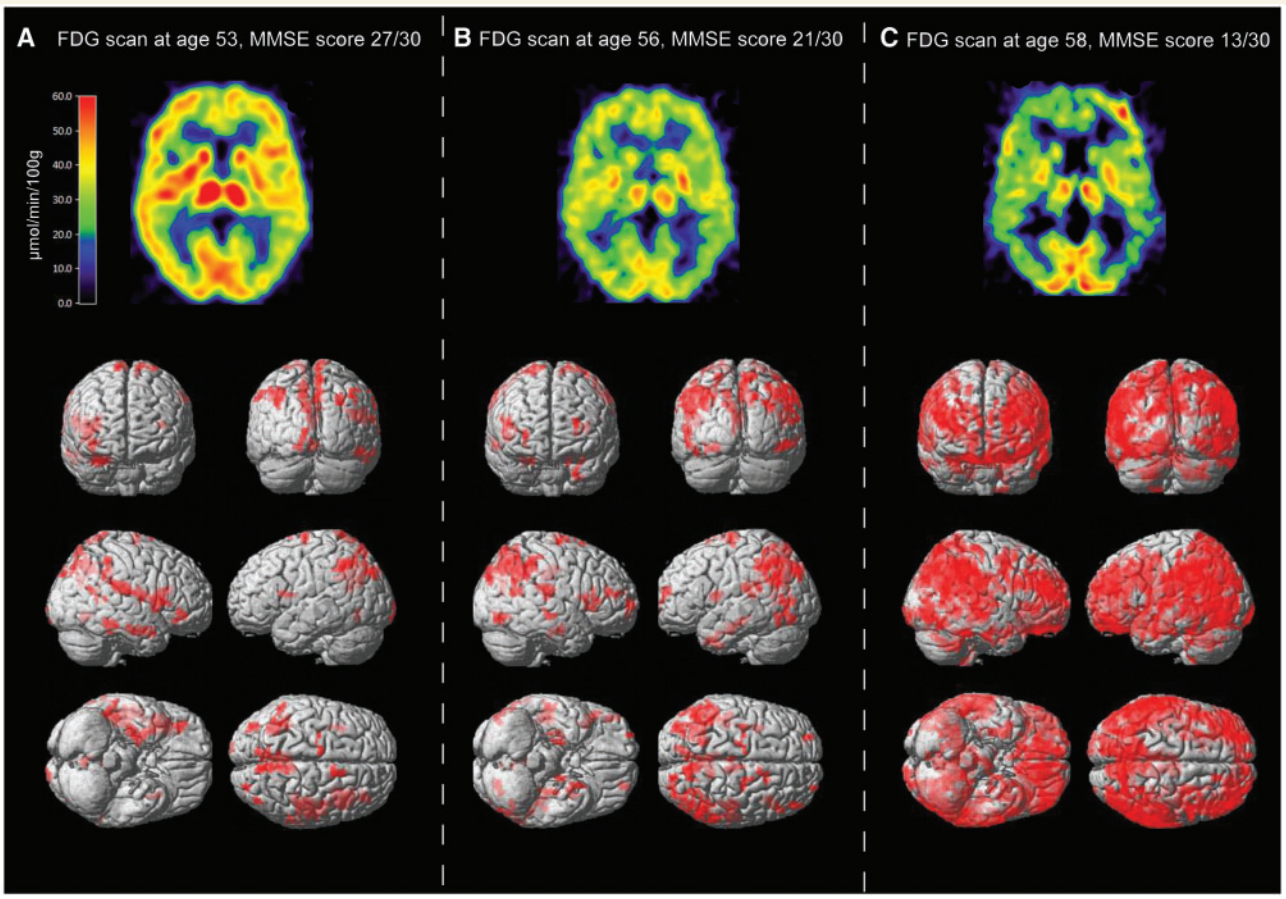

Figure 3 Upper row illustrates the positron emission tomography images of the regional cerebral glucose metabolism (µmol/min/100 g) as measured by ^{18}F-fluorodeoxyglucose (^{18}F-FDG). The coregistered transaxial images are presented at the level of the thalamus at the age of 53 (**A**), 56 (**B**) and 58 (**C**) years. The red colour indicates high, yellow medium and blue low ^{18}F-FDG tracer uptake. Lower row illustrates the 3D brain-rendering representation of statistical parameter mapping of ^{18}F-FDG-PET images. Areas of red depict areas in which the regional cerebral glucose metabolism was significantly decreased in the patient with Alzheimer's disease at the age of 53, 56 and 58 years compared with a group of healthy control subjects ($P = 0.001$, uncorrected, $k = 50$). MMSE = mini-mental state examination.

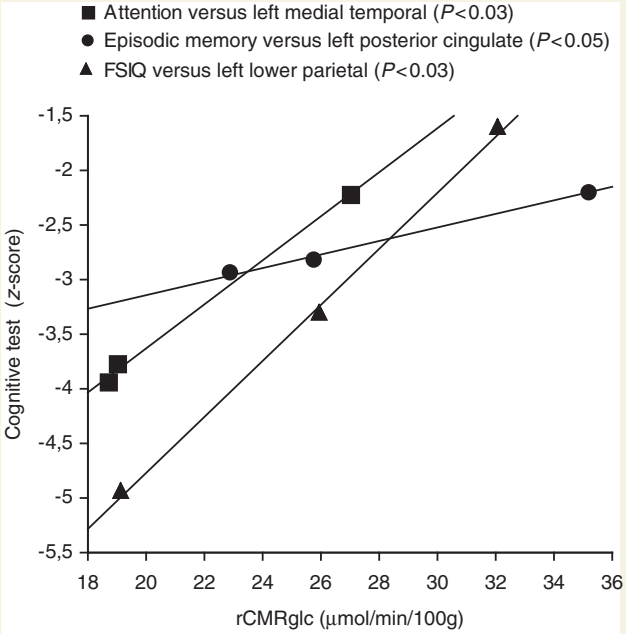

Figure 4 The values of the regional cerebral glucose metabolism (rCMRglc) as measured by ^{18}F-FDG in the left medial temporal, left posterior cingulate and left lower parietal significantly correlated ($P < 0.05$) with attention, episodic memory and Full-Scale Intelligence Quotient tests, respectively, during the time of disease progression (from age 53 to 58 years). Correlation was performed by using the stepwise regression analysis.

+ + + + +) compared to cortical regions (score + + +). Numerous cortical plaques were detected in the parietal cortex (score + + + + + with Aβ1–42 and 6F/3D and score + + + + with 4G8), and the frontal cortex (score + + + + with all three antibodies), consistent with the neuropathological diagnosis (Table 1). In contrast, a diffuse distribution of senile plaques was observed in the hippocampus, striatum, thalamus and cerebellum (ranging in score from + + to – with all antibodies). Neurofibrillary tangles were prominent in the anterior hippocampus (score + + + + +, Fig. 6G and H) and scattered in the frontal, parietal and the occipital lobe cortices. In the hippocampus, an overlap between areas with high tau AT8 immunoreactivity and intracellular 4G8 staining was observed (Table 1). Glial fibrillary acidic protein immunoreactivity was higher in cortical regions in comparison to non-cortical regions and reactive astrocytes were observed in areas with large amounts of amyloid plaque clusters (Fig. 6F). Many of the vessels in the leptomeninges and cortex were stained with the amyloid antibodies. There was a variation in the number of stained vessels with the antibodies used, most abundant with Aβ1–40.

Regional ^{11}C-Pittsburgh Compound B positron emission tomography retention and β-amyloid levels at autopsy

The regional ^{11}C-PIB retention measured by PET, at both 56 and 58 years of age, showed a positive correlation with the regional ^{3}H-PIB binding ($P < 0.001$) as well as the total insoluble Aβ levels ($P < 0.01$) measured in autopsy brain tissue (Fig. 7A and B). A high fibrillar amyloid load visualized with ^{11}C-PIB PET in the frontal and parietal cortex corresponded with the highest measured ^{3}H-PIB binding as well as the highest levels of total insoluble Aβ in these same regions at autopsy.

Across nine brain regions, *in vivo* ^{11}C-PIB retention showed significant positive correlations with semi-quantitative neuropathological assessment of Aβ antibody 6F/3D ($P < 0.001$), Aβ 1–42 ($P < 0.02$) and extracellular Aβ 4G8 ($P < 0.02$) immunoreactivity (Supplementary Fig. 2A–C). Similarly, significant positive correlations were also observed in *in vitro* ^{3}H-PIB binding and 6F/3D ($P < 0.02$), Aβ 1–42 ($P < 0.008$) and extracellular Aβ 4G8 ($P < 0.05$) immunoreactive plaques (Supplementary Fig. 2D–F). No significant correlation was observed between *in vivo* ^{11}C-PIB retention or ^{3}H-PIB binding and intracellular 4G8-stained Aβ.

^{11}C-Pittsburgh Compound B, ^{18}F-fluorodeoxyglucose positron emission tomography and regional distribution of neurofibrillary tangles at autopsy

There was no correlation between regional distribution of *in vivo* ^{11}C-PIB retention or ^{3}H-PIB binding and AT8 tau immunopositive staining for neurofibrillary tangles in autopsy brain (data not shown). A weak non-significant negative correlation ($P < 0.07$) was observed between *in vivo* regional cerebral glucose metabolism as measured by ^{18}F-FDG PET and neurofibrillary tangles (Supplementary Fig. 3), which was driven by the anterior and posterior hippocampus, reflecting the predominance of neurofibrillary tangles in these regions.

^{11}C-Pittsburgh Compound B positron emission tomography retention, ^{3}H-Pittsburgh Compound B and ^{3}H-nicotine binding at autopsy

Figure 8A illustrates the low number of ^{3}H-nicotine binding sites (α4β2 neuronal nicotinic acetylcholine receptors) especially in cortical regions (frontal, parietal and temporal) of the Alzheimer's disease brain in comparison with the regional ^{3}H-nicotine binding in an age-matched control group (historical data from our research laboratory). A weak negative correlation was observed between regional *in vivo* ^{11}C-PIB retention and ^{3}H-nicotine binding at autopsy ($P < 0.06$, Fig. 8B), while a stronger negative correlation was observed between ^{3}H-PIB and ^{3}H-nicotine binding in different brain regions of the autopsy tissue ($P < 0.02$, Fig. 8C). This finding reflects that high fibrillar load is accompanied by a loss of α4β2 neuronal nicotinic acetylcholine receptors in autopsy brain. No significant correlations were observed between *in vivo* ^{11}C-PIB retention or ^{3}H-PIB binding versus ^{125}I-α-bungarotoxin binding (α7-neuronal nicotinic acetylcholine receptors).

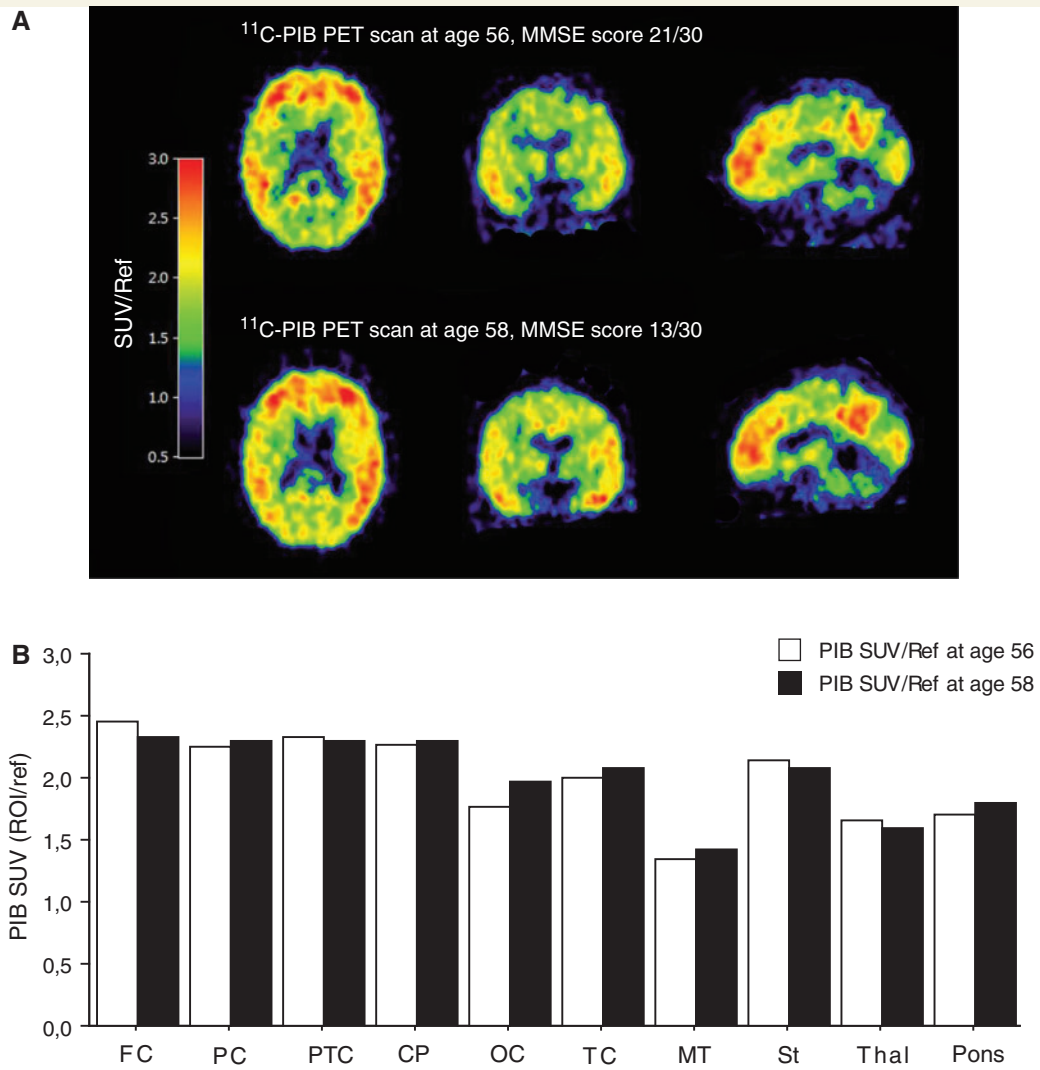

Figure 5 (**A**) ^{11}C-PIB PET scans at 56 and 58 years of age. The ^{11}C-PIB images were derived from dynamic summations of standard uptake values (SUVs) over 40–60 min and were normalized with the cerebellum as a reference region (SUV/Ref). The colour scale indicates red (high), yellow (medium) and blue (low) ^{11}C-PIB retention. The coregistered images represent transaxial, coronal and sagittal sections. (**B**) Comparison of ^{11}C-PIB retention data in two scans in the following brain regions: frontal cortex (FC) (composite of frontal, cingulate anterior and frontal association cortices), parietal cortex (PC) (composite of upper and lower parietal cortices), parietotemporal cortex (PTC), cingulate posterior (CP), occipital cortex (OC), temporal cortex (TC) (composite of temporal inferior and lateral), medial temporal (MT), striatum (St), thalamus (Thal) and pons. With the exception of the pons, all brain regions are the average of the right and left hemisphere. To enable comparison between scans 1 and 2, the standard uptake values were normalized, with the cerebellum as a reference region. MMSE = mini-mental state examination.

Additionally, no correlation was observed between regional cerebral glucose metabolism and ^{3}H-nicotine or ^{125}I-α-bungarotoxin binding, respectively (data not shown).

^{11}C-Pittsburgh Compound B positron emission tomography retention and markers of inflammatory processes at autopsy

A significant positive correlation was observed between regional *in vivo* ^{11}C-PIB PET retention and the total number of glial fibrillary acidic protein immunoreactive cells semiquantitatively assessed in the autopsy brain ($P < 0.03$, Fig. 9A). Significant positive correlations were also found between ^{3}H-PIB binding, extracellular Aβ plaques and the number of glial fibrillary acidic protein immunoreactive cells ($P < 0.01$, Fig. 9B, Table 1).

No significant correlation was observed between ^{11}C-PIB retention or ^{3}H-PIB binding and binding of ^{3}H-PK11195 (activated microglia) and ^{3}H-L-deprenyl (activated astrocytes) in the autopsy brain (data not shown).

A positive correlation was observed between regional ^{3}H-L-deprenyl and ^{3}H-PK11195 binding ($P < 0.03$, Fig. 9C) as well as between ^{3}H-L-deprenyl binding and butyrylcholinesterase activity ($P < 0.02$, Fig. 9D). The highest butyrylcholinesterase activity, as well as the highest binding of ^{3}H-L-deprenyl and

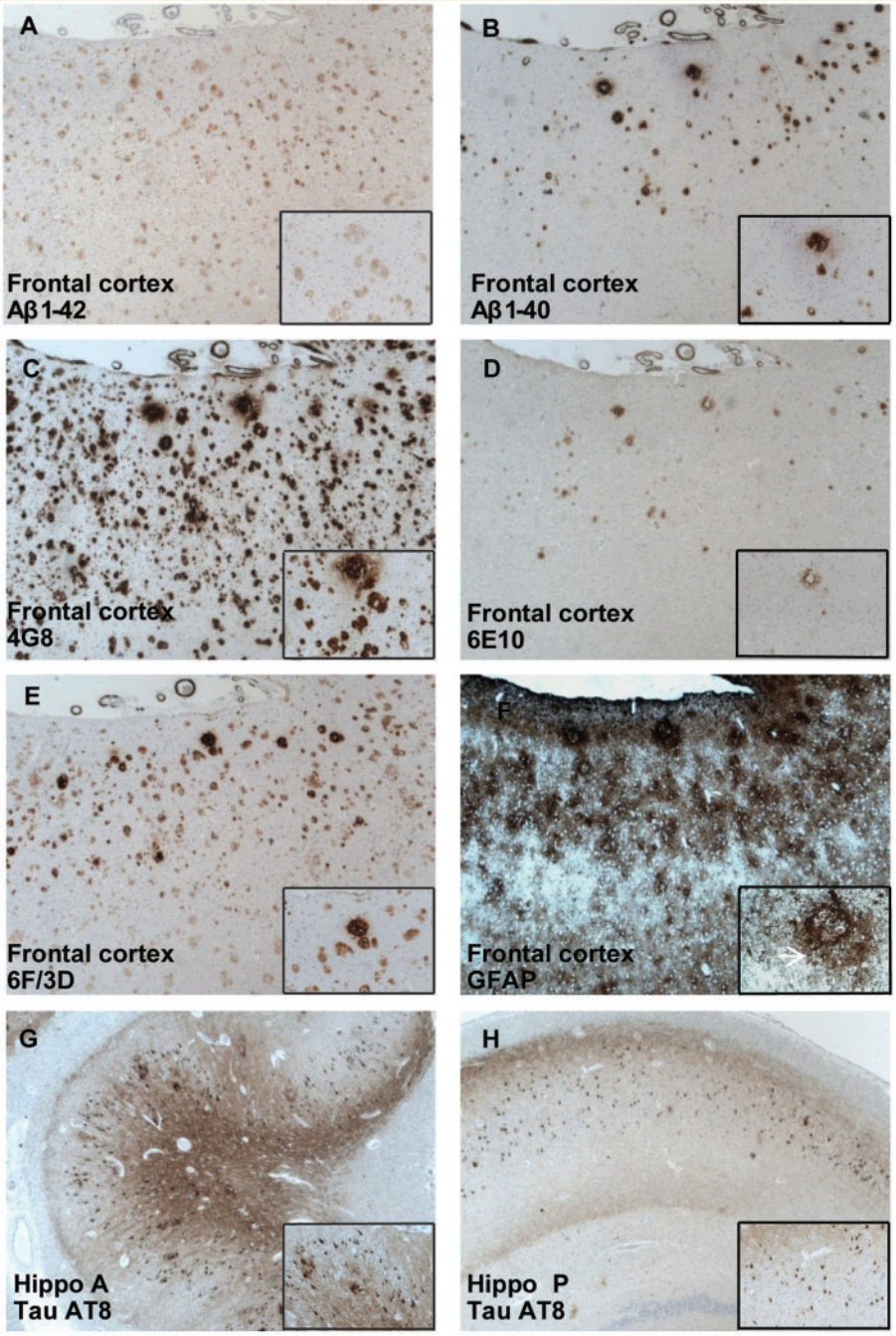

Figure 6 Immunoreactivity in Aβ plaques: (**A**) Aβ1–42, (**B**) Aβ1–40, (**C**) 4G8, (**D**) 6E10 and (**E**) 6F/3D in the frontal cortex. 4G8 immunoreactivity was observed both in extracellular Aβ plaques and in intracellular Aβ deposits (**C**, *bottom right insert*). (**F**) Glial fibrillary acidic protein (GFAP) immunoreactivity in the frontal cortex. Note the round shapes strongly stained for GFAP (reactive astrocytes), as presented in detail and by a white arrow (**F**, *bottom right insert*). (**G**, **H**) AT8 immunoreactivity for tau. A stronger immunoreactivity was detected in the anterior hippocampus (Hippo A) than in the posterior hippocampus (Hippo P) (*bottom right insert*).

^{3}H-PK11195, was observed in the anterior hippocampus in the autopsy brain.

The regional cerebral glucose metabolism did not correlate with either binding of ^{3}H-PK11195, ^{3}H-L-deprenyl or butyrylcholinesterase activity measured at autopsy (data not shown).

None of the neuronal nicotinic acetylcholine receptors subtypes correlated with any of the inflammatory markers studied (data not shown).

Discussion

The significant progress in the field of molecular medicine has advanced our knowledge of the sequence of neurodegenerative events in the brain that lead to dementia disorders such as Alzheimer's disease. The development of different diagnostic biomarkers measuring brain Aβ and regional cerebral glucose

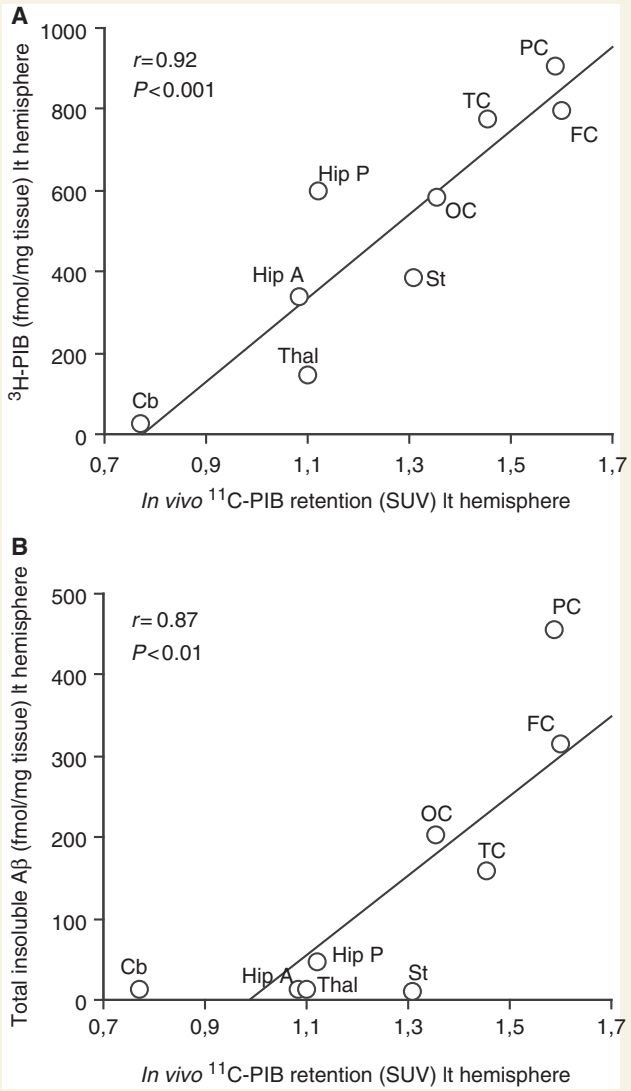

Figure 7 *In vivo* ^{11}C-PIB PET standard uptake values (SUVs) in nine different brain regions of the patient with Alzheimer's disease significantly and positively correlated with (**A**) ^{3}H-PIB binding (fmol/mg tissue) and with (**B**) total insoluble Aβ levels (fmol/mg tissue) measured in autopsy tissue in the corresponding brain regions. In the correlation analysis the following nine brain areas were used: frontal cortex (FC), temporal cortex (TC), parietal cortex (PC), occipital cortex (OC), anterior hippocampus (Hip A), posterior hippocampus (Hip P), striatum (St), thalamus (Thal) and cerebellum (Cb), Left (lt) hemisphere. Note that for the *in vivo* and autopsy correlation analysis, the last ^{11}C-PIB PET scan used was 35 months prior to death.

metabolism by PET, and brain atrophy by MRI as well as CSF biomarkers facilitates the early detection of Alzheimer's disease (Blennow *et al*., 2010; Frisoni *et al*., 2010; Nordberg *et al*., 2010). The clinical benefits of CSF biomarkers and ^{11}C-PIB PET imaging for early diagnosis of prodromal stages of Alzheimer's disease were recently recommended in the National Institute on Ageing-Alzheimer Association draft diagnostic criteria guidelines (http://www.alz.org/reaearch/diagnostic_criteria). While biomarker studies may provide insight into the dynamic relationships between Alzheimer's disease pathology, neurodegeneration and cognition, autopsy studies are important for a secure foundation on which to base further understanding of the cellular and molecular changes that contribute to Alzheimer's disease (Esiri, 2010; Jellinger, 2010).

The patient with Alzheimer's disease described in this study volunteered for the first ^{11}C-PIB PET scan in the world, in February 2002. The patient was clinically followed at regular intervals until her death. Post-mortem neuropathological examination performed 35 months after the last ^{11}C-PIB-PET scan confirmed the clinical diagnosis of Alzheimer's disease with a pure Alzheimer's disease pathology at autopsy. The patient showed a continuous deterioration in cognitive performance, which paralleled the decline in regional cerebral glucose metabolism as observed at three-repeated ^{18}F-FDG scans. Meanwhile, ^{11}C-PIB retention remained stable between baseline and the 2 year follow-up, which is in agreement with reports from other follow-up studies with ^{11}C-PIB in patients with Alzheimer's disease after one year (Jack *et al*., 2009; Scheinin *et al*., 2009), 2 years (Engler *et al*., 2006) and a 5 year follow-up (Kadir *et al*., 2010). In this study, we did not observe any regional correlation between ^{11}C-PIB retention and regional cerebral glucose metabolism. However, previous studies have reported an inverse relation between ^{11}C-PIB retention and regional cerebral glucose metabolism, especially in the parietal cortex (Klunk *et al*., 2004; Engler *et al*., 2006; Edison *et al*., 2007). A high fibrillar Aβ plaque as measured by ^{11}C-PIB was present in this patient with Alzheimer's disease, most notably in cortical regions. We demonstrated that ^{11}C-PIB retention measured by PET at 56 and 58 years of age significantly correlated with region-matched autopsy quantification of Aβ, measured by both ^{3}H-PIB binding and enzyme-linked immunosorbent assay detection of total levels of insoluble Aβ (Aβ40 and Aβ42). Two other studies have reported correlations between *in vivo* ^{11}C-PIB retention and Aβ deposited in autopsy brains (Bacskai *et al*., 2007; Ikonomovic *et al*., 2008). Bacskai *et al*. (2007) studied a case of dementia with Lewy bodies and extensive cerebral Aβ angiopathy, where the ^{11}C-PIB PET imaging had been performed 3 months prior to death. Ikonomovic *et al*. (2008) investigated a patient with Alzheimer's disease with typical clinical symptoms who underwent *in vivo* ^{11}C-PIB-PET imaging, and brain autopsy performed 10 months later. In addition, patients with high fibrillar Aβ levels in frontal cortical biopsy specimens have shown high ^{11}C-PIB retention in the brain 3 years later (Leinonen *et al*., 2008). Altogether, these studies confirm that ^{11}C-PIB retention in the brain is associated with levels of insoluble, but not soluble Aβ. Similar results have been obtained in *in vitro* studies with PIB binding to synthetic Aβ fibrils and insoluble Aβ deposits in human post-mortem brain tissues (Klunk *et al*., 2005; Bacskai *et al*., 2007; Lockhart *et al*., 2007; Ikonomovic *et al*., 2008; Cairns *et al*., 2009; Svedberg *et al*., 2009).

Subsequently, we examined in detail the regional distribution of Aβ plaques in the autopsy brain with immunohistochemistry using five antibodies with different specificity for amino acid residues reactive to the human Aβ peptide. The distribution revealed large extracellular deposits of Aβ plaques in cortical areas that correlated significantly with both ^{11}C-PIB retention measured by

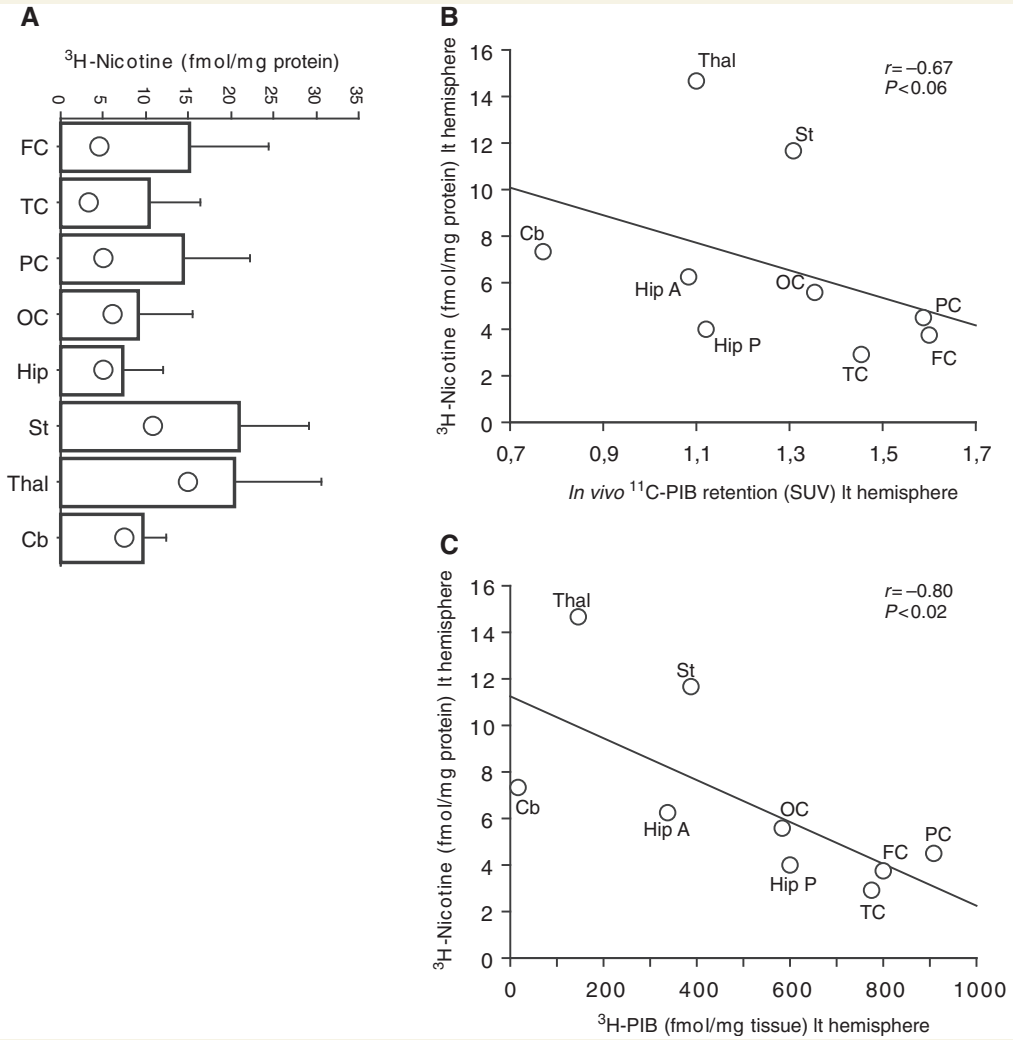

Figure 8 (**A**) Vertical bars (mean ± SD) showing ^{3}H-nicotine binding (fmol/mg protein) in different brain regions in an age-matched control group [historical data collected from our research laboratory; n = 7, mean age: 70 ± 3.1 (SD)]. Open circles within the vertical bars indicates the ^{3}H-nicotine binding (fmol/mg protein) in the same brain regions of the patient with Alzheimer's disease. (**B**) *In vivo* ^{11}C-PIB PET standard uptake values (SUV) and (**C**) *in vitro* ^{3}H-PIB binding (fmol/mg tissue) in the patient with Alzheimer's disease correlated negatively with ^{3}H-nicotine binding (fmol/mg tissue). Nine brain areas in left (lt) hemisphere were analysed for the correlations: frontal cortex (FC), temporal cortex (TC), parietal cortex (PC), occipital cortex (OC), anterior hippocampus (Hip A), posterior hippocampus (Hip P), striatum (St), thalamus (Thal) and cerebellum (Cb).

PET and ^{3}H-PIB binding. Similar labelling of Aβ deposits being detected in sections from human Alzheimer's disease neocortex have been reported in other studies, where investigators used some of the same antibodies applied in this study (Klunk *et al*., 2004; Lockhart *et al*., 2007; Ikonomovic *et al*., 2008).

By using the 4G8 antibody, we found higher intracellular Aβ deposition in the hippocampus than in other brain areas. This observation suggests that there may be differences in the brain regions regarding the internal and external localization of Aβ, as a consequence of the disease state or tissue characteristics. Alternatively, we suggest that these differences observed in 4G8 immunoreactivity could be related to the vulnerability of specific populations of cells in some regions of the brain and to the dynamic relationship between the pools of intracellular and extracellular Aβ. It has been suggested that intracellular accumulation of Aβ interfering with the synaptic activity, occurs prior to extracellular accumulation forming the Aβ plaques (Tampellini and Gouras, 2010). The ^{11}C-PIB retention did not correlate with intracellular Aβ. This probably reflects that PIB binds preferentially to extracellular fibrillar Aβ and less to intracellular Aβ; however future studies investigating this issue as well PIB binding to other forms of Aβ, such as various Aβ oligomers, are warranted.

The hippocampus is a region that typically shows dense neurofibrillary tangle distribution (Thangavel *et al*., 2009), which was evident in this study by the widespread and characteristic distribution pattern of neurofibrillary tangles in this specific region in the autopsy tissue. The reduction of regional cerebral glucose metabolism in susceptible brain regions measured *in vivo* by ^{18}F-FDG

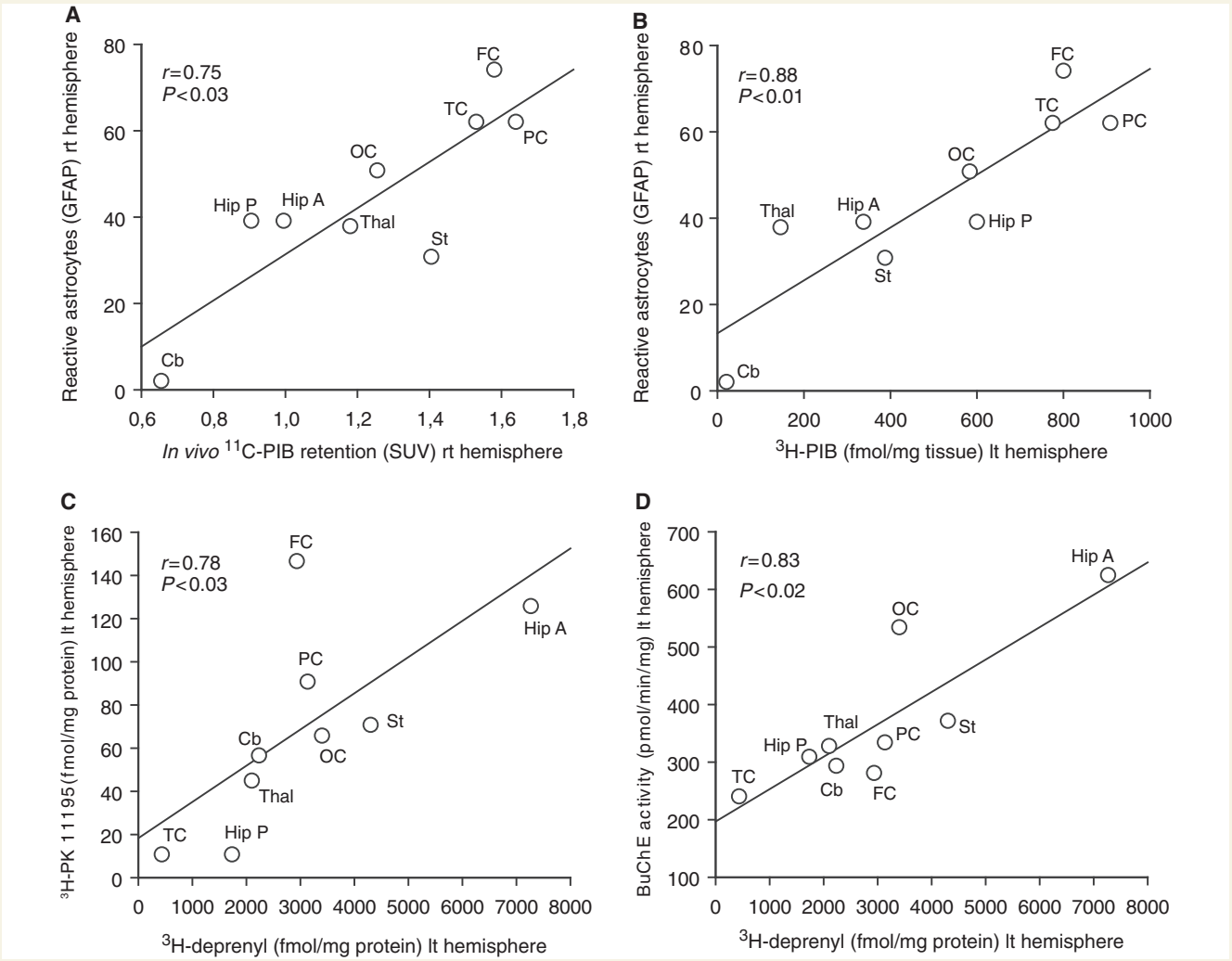

Figure 9 (**A**) Regional brain ^{11}C-PIB retention as measured by PET values, (**B**) ^{3}H-PIB binding (fmol/mg tissue) in the autopsy tissue of the patient with Alzheimer's disease correlated positively with the total number of glia cells as measured by glial fibrillary acidic protein (GFAP) immunoreactivity. (**C**) Positive correlations were found between ^{3}H-L-deprenyl and ^{3}H-PK11195 binding, as measured in different brain regions in the patient with Alzheimer's disease. (**D**) Regional ^{3}H-L-deprenyl binding correlated positively with butyrylcholinesterase activity. Nine brain areas were analysed: frontal cortex (FC), temporal cortex (TC), parietal cortex (PC), occipital cortex (OC), anterior hippocampus (Hip A), posterior hippocampus (Hip P), striatum (St), thalamus (Thal) and cerebellum (Cb). SUV = standard uptake value, rt = right, lt = left.

PET paralleled the finding of an increased number of neurofibrillary tangles in the hippocampus, probably as a marker of neurodegeneration, synaptic activity and clinical progression of Alzheimer's disease (Ingelsson *et al*., 2004; Engler *et al*., 2006; von Gunten *et al*., 2006; Kadir *et al*., 2010). We found no correlation between ^{11}C-PIB retention and the number of neurofibrillary tangles in either the cerebral cortex or the hippocampus, confirming the earlier observation by Ikonomovic *et al*. (2008), who also demonstrated the possibility of PIB binding *in vitro* to a subset of extracellular (ghost) tangles in the entorhinal cortex.

Congo red staining in autopsy brain of this patient with Alzheimer's disease showed several positive vessels in the leptomeninges and the cortex consistent with cerebral amyloid angiopathy, which is commonly observed in patients with Alzheimer's disease. In a series of autopsy cases, covering 117 subjects with clinical Alzheimer's disease, ~80% had demonstrable Aβ deposits within blood vessels, (Ellis *et al*., 1996). The presence of cerebral amyloid angiopathy was higher in patients with Alzheimer's disease having at least one ApoE ε4 allele (Pfeifer *et al*., 2002). It has been shown that ^{3}H-PIB binds to both fibrillar and vascular Aβ (Bacskai *et al*., 2007; Lockhart *et al*., 2007; Ikonomovic *et al*., 2008). In subjects with cerebral amyloid angiopathy, vascular Aβ could be a major contributor to the *in vivo* ^{11}C-PIB signal (Johnson *et al*., 2007; Ly *et al*., 2010). However, cerebral amyloid angiopathy pathology has an occipital predilection, resulting in a greater occipital ^{11}C-PIB retention compared to patients with Alzheimer's disease (Johnson *et al*., 2007; Ly *et al*., 2010). Although we found that Aβ was present in the blood vessels in the autopsy Alzheimer's disease brain, we consider that ^{11}C-PIB binding to cerebral amyloid angiopathy contributed very little to the total *in vivo* ^{11}C-PIB retention.

The impairment of the cholinergic neurotransmitter system is well established in Alzheimer's disease. We have earlier demonstrated significant losses of neuronal nicotinic acetylcholine receptors, especially α4β2 neuronal nicotinic acetylcholine receptors, in autopsy studies of Alzheimer's disease brain tissue as well as by ^{11}C-nicotine PET (Paterson and Nordberg, 2000). Moreover, we have verified with ^{11}C-nicotine PET that the cortical decline in ^{11}C-nicotine binding observed *in vivo* correlates with the cognitive impairment of the patients with Alzheimer's disease (Kadir *et al*., 2006). Reports from several experimental studies also suggest a link between brain neuronal nicotinic acetylcholine receptors and Aβ accumulation in Alzheimer's disease (D'Andrea *et al*., 2001; Dineley *et al*., 2002; Nagele *et al*., 2002; Dougherty *et al*., 2003; Clifford *et al*., 2008). In the present study, we quantified two of the major neuronal nicotinic acetylcholine receptor subtypes (α4β2 and α7 neuronal nicotinic acetylcholine receptors) in different brain regions of the autopsy tissue in the patient with Alzheimer's disease. Low ^{3}H-nicotine binding was measured in brain regions with high ^{11}C-PIB retention, and a strong correlation was found between ^{3}H-PIB and ^{3}H-nicotine binding at autopsy. In an unrelated PET study, including a cohort of seven patients with mild Alzheimer's disease, we observed a significant negative correlation between ^{11}C-PIB retention and ^{11}C-nicotine binding (unpublished observations), which supports our current findings in autopsy brain tissue. The stronger correlation between ^{3}H-nicotine and ^{3}H-PIB at autopsy compared with ^{11}C-PIB *in vivo* may be due to the gradual loss of neuronal nicotinic acetylcholine receptors occurring during Alzheimer's disease progression (neurodegeneration) in comparison to the relatively stable Aβ levels measured by ^{11}C-PIB PET (Nordberg *et al*. 2010). An alternative explanation is that there might be a slight difference in Aβ measured by ^{11}C-PIB compared with ^{3}H-PIB. It is possible that studies with ^{3}H-nicotine binding at autopsy might more readily detect this difference. This new observation regarding α4β2 neuronal nicotinic acetylcholine receptors and fibrillar Aβ is of great interest, and further studies are required to validate this finding and to elucidate the role of neuronal nicotinic acetylcholine receptors in amyloid pathology.

Experimental studies have previously demonstrated that soluble forms of Aβ bind to α7 neuronal nicotinic acetylcholine receptors (Liu *et al*., 2001; Lee and Wang, 2003; Lilja *et al*., 2010). It has previously been shown that the α7 neuronal nicotinic acetylcholine receptors are present both on neurons as well as on glia cells, and these receptors have been reported to be reduced on neurons in autopsy brain tissue from patients with Alzheimer's disease (Yu *et al*., 2005) and increased on astrocytes (Teaktong *et al*., 2003; Yu *et al*., 2005). Although an increased number of α7 neuronal nicotinic acetylcholine receptors in autopsy brain tissue from patients with Alzheimer's disease with high Aβ load in brain was recently reported (Ikonomovic *et al*., 2009), we did not observe any correlation between either regional ^{11}C-PIB retention *in vivo* or ^{3}H-PIB and α7 neuronal nicotinic acetylcholine receptors as measured by ^{125}I-α-bungarotoxin binding in the present study. It may be difficult in tissue homogenates to distinguish between α7 neuronal nicotinic acetylcholine receptors localized on neurons versus astrocytes, which could be a possible explanation as to why we did not observe any correlation with fibrillar Aβ levels.

The consequence and the time course of inflammatory processes, in relation to fibrillar Aβ during the progression of Alzheimer's disease, are still under investigation. Increased numbers of both activated microglial cells and reactive astrocytes are often observed in the vicinity of the fibrillar core of Aβ plaques in the Alzheimer's disease autopsy brain (Braak *et al*., 1998; Zhu *et al*., 1999). These observations suggest that the increase in activated microglia and activated astrocytes may reflect attempts by these glial cells to clear Aβ in the brain. However, when the disease progresses, they may instead potentiate neurotoxicity by releasing toxic immune mediators (McGeer *et al*., 2000).

Increased binding of ^{3}H-PK-11195, a peripheral-type benzodiazepine binding site ligand, has been measured in homogenates from Alzheimer's disease brains reflecting an increase in microglia/macrophages (Diorio *et al*., 1991; Saura *et al*., 1994). Similarly, increased monoamine oxidase B activity has been measured in Aβ plaque-associated astrocytes with other monoamine oxidase B ligands such as ^{3}H-lazabemide (Saura *et al*., 1994) and ^{3}H L-deprenyl (Jossan *et al*., 1991*b*). Both ^{11}C-PK11195 and ^{11}C-L-deuterodeprenyl have been used as PET ligands for visualizing activated microglia and astrocytes, respectively (Cagnin *et al*., 2001; Engler *et al*., 2003) in neurodegenerative diseases. While a strong binding signal of these tracers is detected in multiple sclerosis (Debruyne *et al*., 2003) and Creutzfeldt-Jacob disease (Engler *et al*., 2003), the ^{11}C-PK11195 binding has varied in Alzheimer's disease in different PET studies. Increased binding of ^{11}C-PK11195 was reported in cortical regions of patients with mild Alzheimer's disease when compared with healthy controls (Cagnin *et al*., 2001). In more recent PET studies, low ^{11}C-PK1195 binding was measured in patients with Alzheimer's disease and mild cognitive impairment (Okello *et al*., 2009; Wiley *et al*., 2009). Increased ^{11}C-PK1195 binding was observed by Edison *et al*. (2008) in regions associated with high ^{11}C-PIB retention, further demonstrating an inverse correlation between cognition and levels of cortical ^{11}C-PK1195 binding measured by PET. In a recent PET study in patients with mild cognitive impairment, the investigators did not find such a correlation between ^{11}C-PK11195 and ^{11}C-PIB retention (Okello *et al*., 2009). Similarly, we did not observe any relation between ^{11}C-PIB retention or ^{3}H-PIB and ^{3}H-PK1195 binding in the present study. A possible explanation for these different findings with ^{11}C-PK11195 might be changes in binding affinity during different stages of microglia activation (Vas *et al*., 2008).

In the current study, a positive correlation was found between glial fibrillary acidic protein immunopositive cells and *in vivo* ^{11}C-PIB retention as well as ^{3}H-PIB binding and extracellular Aβ quantified by immunohistochemistry. This finding supports the assumption that astrocytosis is located in close proximity to fibrillar Aβ plaque formation (Simpson *et al*., 2010). A positive correlation has been demonstrated between ^{3}H-lazabemide (monoamine oxidase B inhibitor) and glial fibrillary acidic protein immunoreactivity in the Alzheimer's disease brain (Saura *et al*., 1994). We found no relationship between regional ^{11}C-PIB retention or ^{3}H-PIB binding and ^{3}H-L-deprenyl binding in the autopsy brain. The lack of a correlation between ^{3}H-L-deprenyl binding and fibrillar Aβ might reflect low binding of ^{3}H-L-deprenyl to monoamine oxidase B in autopsy brain tissue. This does not exclude the use of ^{11}C-L-deuterodeprenyl as an *in vivo* PET tracer for detecting

early changes in activated astrocytes. In support, we have recently observed an increase in ^{11}C-L-deuterodeprenyl binding in patients with mild cognitive impairment and mild Alzheimer's disease compared to controls (Carter *et al*., 2010). No correlation was observed between regional changes in ^{11}C-L-deuterodeprenyl binding and ^{11}C-PIB retention or regional cerebral glucose metabolism, respectively (Carter *et al*., 2010).

In the present study, we found a positive correlation between regional ^{3}H-L-deprenyl and butyrylcholinesterase activity, probably reflecting a pathophysiological consequence of butyrylcholinesterase activity on inflammatory processes in the Alzheimer's disease brain (Darreh-Shori *et al*., 2009). An increased brain butyrylcholinesterase activity has been attributed to an increase in the prevalence of reactive glial cells and Aβ plaques, to which this enzyme is localized (Perry *et al*., 1978; Geula and Mesulam, 1995; Lehmann *et al*., 2000; Tasker *et al*., 2005). We have recently observed a strong positive correlation between CSF butyrylcholinesterase activity and cortical ^{11}C-PIB retention (Darreh-Shori *et al*., 2010). Interestingly, ^{3}H-L-deprenyl, ^{3}H-PK11195 and butyrylcholinesterase all showed high binding and activity in the hippocampus, a region characterized by a high amount of neurofibrillary tangles as a sign for neurodegenerative processes.

In conclusion, this study confirmed the pure Alzheimer's disease pathology of the first ^{11}C-PIB PET imaged patient with Alzheimer's disease. We demonstrated a strong correlation between fibrillar Aβ measured by PET and at autopsy several years later. Loss of neuronal nicotinic acetylcholine receptors (α4β2 subtype) at autopsy was associated with high levels of fibrillar Aβ, suggesting that neuronal nicotinic acetylcholine receptors, as markers for degenerative processes, may closely be linked to Aβ pathology. Although, we found a positive correlation between glial fibrillary acidic protein immunoreactivity and fibrillar Aβ, measured by PET as well as at autopsy, the lack of a correlation between fibrillar Aβ and binding of the two PET tracers PK11195 and deprenyl in autopsy tissue, suggests that these tracers should further be studied *in vivo* by PET in order to gain a better understanding of the time course for early changes in neuroinflammatory processes in relation to Aβ in Alzheimer's disease.

Acknowledgements

The authors thank Dr Lena Cavallin (Department of Radiology, Karolinska University Hospital Huddinge, Stockholm) for evaluation of the MRI scan and Dr Anders Wall (Uppsala PET Centre/Uppsala Imanet AB) for his assistance with preparing PET figures. We also express our sincere gratitude to the patient and her relatives for participation and permission to accomplish this study. Finally, we will dedicate this study to the memory of the patient.

Funding

Swedish Research Council (project 05817); Swedish Brain Power; Stockholm County Council-Karolinska Institutet (ALF grant); the Karolinska Institutet Strategic Neuroscience Program; the EC-FP6 project DiMI, LSHB-CT-2005-512146; the Swedish Brain Foundation; the Alzheimer Foundation in Sweden; the Magnus Bergvalls Foundation; Demensfonden, the foundation for Old Servants; Gun and Bertil Stohnes Foundation; Karolinska Institutet foundations; the Lars Hierta Memorial Foundation; Olle Engkvist Byggmästare Foundation.

Supplementary material

Supplementary material is available at *Brain* online.

References

Alafuzoff I, Pikkarainen M, Al-Sarraj S, Arzberger T, Bell J, Bodi I, et al. Interlaboratory comparison of assessments of Alzheimer disease-related lesions: a study of the BrainNet Europe Consortium. J Neuropathol Exp Neurol 2006; 65: 740–57.

Almkvist O, Tallberg IM. Cognitive decline from estimated premorbid status predicts neurodegeneration in Alzheimer's disease. Neuropsychology 2009; 23: 117–24.

Andersson JL, Thurfjell L. Implementation and validation of a fully automatic system for intra- and interindividual registration of PET brain scans. J Comput Assist Tomogr 1997; 21: 136–44.

Bacskai BJ, Frosch MP, Freeman SH, Raymond SB, Augustinack JC, Johnson KA, et al. Molecular imaging with Pittsburgh Compound B confirmed at autopsy: a case report. Arch Neurol 2007; 64: 431–4.

Bergman I, Blomberg M, Almkvist O. The importance of impaired physical health and age in normal cognitive aging. Scand J Psychol 2007; 48: 115–25.

Blennow K, Hampel H, Weiner M, Zetterberg H. Cerebrospinal fluid and plasma biomarkers in Alzheimer disease. Nat Rev Neurol 2010; 6: 131–44.

Braak H, Braak E. Neuropathological stageing of Alzheimer-related changes. Acta Neuropathol 1991; 82: 239–59.

Braak H, de Vos RA, Jansen EN, Bratzke H, Braak E. Neuropathological hallmarks of Alzheimer's and Parkinson's diseases. Prog Brain Res 1998; 117: 267–85.

Cagnin A, Brooks DJ, Kennedy AM, Gunn RN, Myers R, Turkheimer FE, et al. In-vivo measurement of activated microglia in dementia. Lancet 2001; 358: 461–7.

Cairns NJ, Ikonomovic MD, Benzinger T, Storandt M, Fagan AM, Shah A, et al. Absence of PIttsburgh compound B detection of cerebral amyloid beta in a patient with clinical, cognitive, and cerebrospinal fluid markers of Alzheimer disease. Arch Neurol 2009; 66: 1557–62.

Carter SF, Schöll M, Almkvist O, Wall A, Engler H, Långström B, et al. Investigating astrocytes with ^{11}C-deuterium deprenyl in mild cognitive impairment and mild Alzheimer's - a multi-tracer positron emission tomography paradigm. The abstract/poster (poster number P4-089) was presented in the Hot Topics session in Alzheimer's Association International Conference on Alzheimer's Disease 2010 (AAICAD), July 10–15, Honolulu, Hawaii. 2010.

Clifford PM, Siu G, Kosciuk M, Levin EC, Venkataraman V, D'Andrea MR, et al. Alpha7 nicotinic acetylcholine receptor expression by vascular smooth muscle cells facilitates the deposition of Abeta peptides and promotes cerebrovascular amyloid angiopathy. Brain Res 2008; 1234: 158–71.

Cummings BJ, Pike CJ, Shankle R, Cotman CW. Beta-amyloid deposition and other measures of neuropathology predict cognitive status in Alzheimer's disease. Neurobiol Aging 1996; 17: 921–33.

D'Andrea MR, Nagele RG, Wang HY, Peterson PA, Lee DH. Evidence that neurones accumulating amyloid can undergo lysis to form amyloid plaques in Alzheimer's disease. Histopathology 2001; 38: 120–34.

Darreh-Shori T, Brimijoin S, Kadir A, Almkvist O, Nordberg A. Differential CSF butyrylcholinesterase levels in Alzheimer's disease patients with

the ApoE epsilon4 allele, in relation to cognitive function and cerebral glucose metabolism. Neurobiol Dis 2006; 24: 326–33.

Darreh-Shori T, Forsberg A, Modiri N, Andreasen N, Blennow K, Kamil C, et al. Differential levels of apolipoprotein E and butyrylcholinesterase show strong association with pathological signs of Alzheimer's disease in the brain in vivo. Neurobiol Aging 2010. Advance Access published on June 8, 2010, doi:10.1016/j.neurobiolaging.2010.04.028.

Darreh-Shori T, Modiri N, Blennow K, Baza S, Kamil C, Ahmed H, et al. The apolipoprotein E varepsilon4 allele plays pathological roles in AD through high protein expression and interaction with butyrylcholinesterase. Neurobiol Aging 2009. doi:10.1016/j.neurobiolaging.2009.07.015, (published online 25 August 2009).

Debruyne JC, Versijpt J, Van Laere KJ, De Vos F, Keppens J, Strijckmans K, et al. PET visualization of microglia in multiple sclerosis patients using [11C]PK11195. Eur J Neurol 2003; 10: 257–64.

Dineley KT, Bell KA, Bui D, Sweatt JD. beta -Amyloid peptide activates alpha 7 nicotinic acetylcholine receptors expressed in Xenopus oocytes. J Biol Chem 2002; 277: 25056–61.

Diorio D, Welner SA, Butterworth RF, Meaney MJ, Suranyi-Cadotte BE. Peripheral benzodiazepine binding sites in Alzheimer's disease frontal and temporal cortex. Neurobiol Aging 1991; 12: 255–8.

Dougherty JJ, Wu J, Nichols RA. Beta-amyloid regulation of presynaptic nicotinic receptors in rat hippocampus and neocortex. J Neurosci 2003; 23: 6740–7.

Edison P, Archer HA, Gerhard A, Hinz R, Pavese N, Turkheimer FE, et al. Microglia, amyloid, and cognition in Alzheimer's disease: An [11C](R)PK11195-PET and [11C]PIB-PET study. Neurobiol Dis 2008; 32: 412–9.

Edison P, Archer HA, Hinz R, Hammers A, Pavese N, Tai YF, et al. Amyloid, hypometabolism, and cognition in Alzheimer disease: an [11C]PIB and [18F]FDG PET study. Neurology 2007; 68: 501–8.

Ellis RJ, Olichney JM, Thal LJ, Mirra SS, Morris JC, Beekly D, et al. Cerebral amyloid angiopathy in the brains of patients with Alzheimer's disease: the CERAD experience, Part XV. Neurology 1996; 46: 1592–6.

Engler H, Forsberg A, Almkvist O, Blomquist G, Larsson E, Savitcheva I, et al. Two-year follow-up of amyloid deposition in patients with Alzheimer's disease. Brain 2006; 129: 2856–66.

Engler H, Lundberg PO, Ekbom K, Nennesmo I, Nilsson A, Bergstrom M, et al. Multitracer study with positron emission tomography in Creutzfeldt-Jakob disease. Eur J Nucl Med Mol Imaging 2003; 30: 85–95.

Esiri MM. Pro: can neuropathology really confirm the exact diagnosis? Alzheimers Res Ther 2010; 2: 10.

Forsberg A, Almkvist O, Engler H, Wall A, Langstrom B, Nordberg A. High PIB retention in Alzheimer's disease is an early event with complex relationship with CSF biomarkers and functional parameters. Curr Alzheimer Res 2010; 7: 56–66.

Forsberg A, Engler H, Almkvist O, Blomquist G, Hagman G, Wall A, et al. PET imaging of amyloid deposition in patients with mild cognitive impairment. Neurobiol Aging 2008; 29: 1456–65.

Frisoni GB, Fox NC, Jack CR Jr, Scheltens P, Thompson PM. The clinical use of structural MRI in Alzheimer disease. Nat Rev Neurol 2010; 6: 67–77.

Furst AJ, Rabinovici GD, Rostomian AH, Steed T, Alkalay A, Racine C, et al. Cognition, glucose metabolism and amyloid burden in Alzheimer's disease. Neurobiol Aging 2010. Advance Access published on April 22, 2010, doi:10.1016/j.neurobiolaging.2010.03.011.

Geula C, Mesulam MM. Cholinesterases and the pathology of Alzheimer disease. Alzheimer Dis Assoc Disord 1995; 9 (Suppl 2): 23–8.

Guan ZZ, Miao H, Tian JY, Unger C, Nordberg A, Zhang X. Suppressed expression of nicotinic acetylcholine receptors by nanomolar beta-amyloid peptides in PC12 cells. J Neural Transm 2001; 108: 1417–33.

Hellstrom-Lindahl E, Mousavi M, Ravid R, Nordberg A. Reduced levels of Abeta 40 and Abeta 42 in brains of smoking controls and Alzheimer's patients. Neurobiol Dis 2004; 15: 351–60.

Ikonomovic MD, Klunk WE, Abrahamson EE, Mathis CA, Price JC, Tsopelas ND, et al. Post-mortem correlates of in vivo PiB-PET amyloid imaging in a typical case of Alzheimer's disease. Brain 2008; 131: 1630–45.

Ikonomovic MD, Wecker L, Abrahamson EE, Wuu J, Counts SE, Ginsberg SD, et al. Cortical alpha7 nicotinic acetylcholine receptor and beta-amyloid levels in early Alzheimer disease. Arch Neurol 2009; 66: 646–51.

Ingelsson M, Fukumoto H, Newell KL, Growdon JH, Hedley-Whyte ET, Frosch MP, et al. Early Abeta accumulation and progressive synaptic loss, gliosis, and tangle formation in AD brain. Neurology 2004; 62: 925–31.

Jack CR Jr, Lowe VJ, Weigand SD, Wiste HJ, Senjem ML, Knopman DS, et al. Serial PIB and MRI in normal, mild cognitive impairment and Alzheimer's disease: implications for sequence of pathological events in Alzheimer's disease. Brain 2009; 132: 1355–65.

Jellinger KA. Con: can neuropathology really confirm the exact diagnosis? Alzheimers Res Ther 2010; 2: 11.

Johnson KA, Gregas M, Becker JA, Kinnecom C, Salat DH, Moran EK, et al. Imaging of amyloid burden and distribution in cerebral amyloid angiopathy. Ann Neurol 2007; 62: 229–34.

Jossan SS, Gillberg PG, d'Argy R, Aquilonius SM, Langstrom B, Halldin C, et al. Quantitative localization of human brain monoamine oxidase B by large section autoradiography using L-[3H]deprenyl. Brain Res 1991a; 547: 69–76.

Jossan SS, Gillberg PG, Gottfries CG, Karlsson I, Oreland L. Monoamine oxidase B in brains from patients with Alzheimer's disease: a biochemical and autoradiographical study. Neuroscience 1991b; 45: 1–12.

Kadir A, Almkvist O, Forsberg A, Wall A, Engler H, Langstrom B, et al. Dynamic changes in PET amyloid and FDG imaging at different stages of Alzheimer's disease. Neurobiol Aging 2010. Advance Access published on August 3, 2010, doi:10.1016/j.neurobiolaging.2010.06.015.

Kadir A, Almkvist O, Wall A, Langstrom B, Nordberg A. PET imaging of cortical 11C-nicotine binding correlates with the cognitive function of attention in Alzheimer's disease. Psychopharmacology 2006; 188: 509–20.

Klunk WE, Engler H, Nordberg A, Wang Y, Blomqvist G, Holt DP, et al. Imaging brain amyloid in Alzheimer's disease with Pittsburgh Compound-B. Ann Neurol 2004; 55: 306–19.

Klunk WE, Lopresti BJ, Ikonomovic MD, Lefterov IM, Koldamova RP, Abrahamson EE, et al. Binding of the positron emission tomography tracer Pittsburgh compound-B reflects the amount of amyloid-beta in Alzheimer's disease brain but not in transgenic mouse brain. J Neurosci 2005; 25: 10598–606.

Kumlien E, Hilton-Brown P, Spannare B, Gillberg PG. In vitro quantitative autoradiography of [3H]-L-deprenyl and [3H]-PK 11195 binding sites in human epileptic hippocampus. Epilepsia 1992; 33: 610–7.

Lee DH, Wang HY. Differential physiologic responses of alpha7 nicotinic acetylcholine receptors to beta-amyloid1-40 and beta-amyloid1-42. J Neurobiol 2003; 55: 25–30.

Lehmann DJ, Nagy Z, Litchfield S, Borja MC, Smith AD. Association of butyrylcholinesterase K variant with cholinesterase-positive neuritic plaques in the temporal cortex in late-onset Alzheimer's disease. Hum Genet 2000; 106: 447–52.

Leinonen V, Alafuzoff I, Aalto S, Suotunen T, Savolainen S, Nagren K, et al. Assessment of beta-amyloid in a frontal cortical brain biopsy specimen and by positron emission tomography with carbon 11-labeled Pittsburgh Compound B. Arch Neurol 2008; 65: 1304–9.

Lilja AM, Porras O, Storelli E, Nordberg A, Marutle A. Functional interactions of fibrillar and oligomeric amyloid β with alpha 7 nicotinic receptors in Alzheimer's disease. doi:10.3233/j. Alzheimer's Dis.2010-101242; In press.

Liu Y, Ford B, Mann MA, Fischbach GD. Neuregulins increase alpha7 nicotinic acetylcholine receptors and enhance excitatory synaptic transmission in GABAergic interneurons of the hippocampus. J Neurosci 2001; 21: 5660–9.

Lockhart A, Lamb JR, Osredkar T, Sue LI, Joyce JN, Ye L, et al. PIB is a non-specific imaging marker of amyloid-beta (Abeta) peptide-related cerebral amyloidosis. Brain 2007; 130: 2607–15.

Ly JV, Donnan GA, Villemagne VL, Zavala JA, Ma H, O'Keefe G, et al. 11C-PIB binding is increased in patients with cerebral amyloid angiopathy-related hemorrhage. Neurology 2010; 74: 487–93.

Marutle A, Warpman U, Bogdanovic N, Nordberg A. Regional distribution of subtypes of nicotinic receptors in human brain and effect of aging studied by (+/-)-[3H]epibatidine. Brain Res 1998; 801: 143–9.

Mathis CA, Wang Y, Holt DP, Huang GF, Debnath ML, Klunk WE. Synthesis and evaluation of 11C-labeled 6-substituted 2-arylbenzothiazoles as amyloid imaging agents. J Med Chem 2003; 46: 2740–54.

Mattson MP. Pathways towards and away from Alzheimer's disease. Nature 2004; 430: 631–9.

McGeer PL, McGeer EG, Yasojima K. Alzheimer disease and neuroinflammation. J Neural Transm Suppl 2000; 59: 53–7.

McKhann G, Drachman D, Folstein M, Katzman R, Price D, Stadlan EM. Clinical diagnosis of Alzheimer's disease: report of the NINCDS-ADRDA Work Group under the auspices of Department of Health and Human Services Task Force on Alzheimer's Disease. Neurology 1984; 34: 939–44.

Mirra SS, Gearing M, McKeel DW Jr, Crain BJ, Hughes JP, van Belle G, et al. Interlaboratory comparison of neuropathology assessments in Alzheimer's disease: a study of the Consortium to Establish a Registry for Alzheimer's Disease (CERAD). J Neuropathol Exp Neurol 1994; 53: 303–15.

Mirra SS, Heyman A, McKeel D, Sumi SM, Crain BJ, Brownlee LM, et al. The Consortium to Establish a Registry for Alzheimer's Disease (CERAD). Part II. Standardization of the neuropathologic assessment of Alzheimer's disease. Neurology 1991; 41: 479–86.

Nagele RG, D'Andrea MR, Anderson WJ, Wang HY. Intracellular accumulation of beta-amyloid(1-42) in neurons is facilitated by the alpha 7 nicotinic acetylcholine receptor in Alzheimer's disease. Neuroscience 2002; 110: 199–211.

Nordberg A. Nicotinic receptor abnormalities of Alzheimer's disease: therapeutic implications. Biol Psychiatry 2001; 49: 200–10.

Nordberg A, Rinne JO, Kadir A, Langstrom B. The use of PET in Alzheimer disease. Nat Rev Neurol 2010; 6: 78–87.

Okello A, Edison P, Archer HA, Turkheimer FE, Kennedy J, Bullock R, et al. Microglial activation and amyloid deposition in mild cognitive impairment: a PET study. Neurology 2009; 72: 56–62.

Paterson D, Nordberg A. Neuronal nicotinic receptors in the human brain. Prog Neurobiol 2000; 61: 75–111.

Patlak CS, Blasberg RG, Fenstermacher JD. Graphical evaluation of blood-to-brain transfer constants from multiple-time uptake data. J Cereb Blood Flow Metab 1983; 3: 1–7.

Perry EK, Perry RH, Blessed G, Tomlinson BE. Changes in brain cholinesterases in senile dementia of Alzheimer type. Neuropathol Appl Neurobiol 1978; 4: 273–7.

Pfeifer LA, White LR, Ross GW, Petrovitch H, Launer LJ. Cerebral amyloid angiopathy and cognitive function: the HAAS autopsy study. Neurology 2002; 58: 1629–34.

Price JL, McKeel DW Jr, Buckles VD, Roe CM, Xiong C, Grundman M, et al. Neuropathology of nondemented aging: presumptive evidence for preclinical Alzheimer disease. Neurobiol Aging 2009; 30: 1026–36.

Saura J, Luque JM, Cesura AM, Da Prada M, Chan-Palay V, Huber G, et al. Increased monoamine oxidase B activity in plaque-associated astrocytes of Alzheimer brains revealed by quantitative enzyme radioautography. Neuroscience 1994; 62: 15–30.

Scheinin NM, Aalto S, Koikkalainen J, Lotjonen J, Karrasch M, Kemppainen N, et al. Follow-up of [11C]PIB uptake and brain volume in patients with Alzheimer disease and controls. Neurology 2009; 73: 1186–92.

Scheltens P, Leys D, Barkhof F, Huglo D, Weinstein HC, Vermersch P, et al. Atrophy of medial temporal lobes on MRI in "probable" Alzheimer's disease and normal ageing: diagnostic value and neuropsychological correlates. J Neurol Neurosurg Psychiatry 1992; 55: 967–72.

Schöll M, Almkvist O, Axelman K, Stefanova E, Wall A, Westman E, et al. Glucose metabolism and PIB binding in carriers of a His163Tyr presenilin 1 mutation. Neurobiol Aging 2009. Advance Access published on September 29, 2009, doi:10.1016/j.neurobiolaging.2009.08.016.

Simpson JE, Ince PG, Lace G, Forster G, Shaw PJ, Matthews F, et al. Astrocyte phenotype in relation to Alzheimer-type pathology in the ageing brain. Neurobiol Aging 2010; 31: 578–90.

Svedberg MM, Hall H, Hellstrom-Lindahl E, Estrada S, Guan Z, Nordberg A, et al. [(11)C]PIB-amyloid binding and levels of Abeta40 and Abeta42 in postmortem brain tissue from Alzheimer patients. Neurochem Int 2009; 54: 347–57.

Talairach J, Tournoux P. Co-planar Stereotaxic Atlas of the Human Brain. New York: Thieme Medical; 1988.

Tampellini D, Gouras GK. Synapses, synaptic activity and intraneuronal abeta in Alzheimer's disease. Front Aging Neurosci 2010; 2: 1–5.

Tasker A, Perry EK, Ballard CG. Butyrylcholinesterase: impact on symptoms and progression of cognitive impairment. Expert Rev Neurother 2005; 5: 101–6.

Teaktong T, Graham A, Court J, Perry R, Jaros E, Johnson M, et al. Alzheimer's disease is associated with a selective increase in alpha7 nicotinic acetylcholine receptor immunoreactivity in astrocytes. Glia 2003; 41: 207–11.

Thal DR, Rub U, Orantes M, Braak H. Phases of A beta-deposition in the human brain and its relevance for the development of AD. Neurology 2002; 58: 1791–800.

Thangavel R, Van Hoesen GW, Zaheer A. The abnormally phosphorylated tau lesion of early Alzheimer's disease. Neurochem Res 2009; 34: 118–23.

Vas A, Shchukin Y, Karrenbauer VD, Cselenyi Z, Kostulas K, Hillert J, et al. Functional neuroimaging in multiple sclerosis with radiolabelled glia markers: preliminary comparative PET studies with [11C]vinpocetine and [11C]PK11195 in patients. J Neurol Sci 2008; 264: 9–17.

Wiley CA, Lopresti BJ, Venneti S, Price J, Klunk WE, DeKosky ST, et al. Carbon 11-labeled Pittsburgh Compound B and carbon 11-labeled (R)-PK11195 positron emission tomographic imaging in Alzheimer disease. Arch Neurol 2009; 66: 60–7.

von Gunten A, Kovari E, Bussiere T, Rivara CB, Gold G, Bouras C, et al. Cognitive impact of neuronal pathology in the entorhinal cortex and CA1 field in Alzheimer's disease. Neurobiol Aging 2006; 27: 270–7.

Yamaguchi H, Hirai S, Morimatsu M, Shoji M, Nakazato Y. Diffuse type of senile plaques in the cerebellum of Alzheimer-type dementia demonstrated by beta protein immunostain. Acta Neuropathol 1989; 77: 314–9.

Yu WF, Guan ZZ, Bogdanovic N, Nordberg A. High selective expression of alpha7 nicotinic receptors on astrocytes in the brains of patients with sporadic Alzheimer's disease and patients carrying Swedish APP 670/671 mutation: a possible association with neuritic plaques. Exp Neurol 2005; 192: 215–25.

Zhu SG, Sheng JG, Jones RA, Brewer MM, Zhou XQ, Mrak RE, et al. Increased interleukin-1beta converting enzyme expression and activity in Alzheimer disease. J Neuropathol Exp Neurol 1999; 58: 582–7.